ACS OMEGA

Article

Cite This: ACS Omega 2018, 3, 3991−4005

# Functionalized Hydrophilic Superparamagnetic Iron Oxide Nanoparticles for Magnetic Fluid Hyperthermia Application in Liver Cancer Treatment

Ganeshlenin Kandasamy,[†] Atul Sudame,[†] Tania Luthra,[‡] Kalawati Saini,[§] and Dipak Maity*[,†]

[†]Department of Mechanical Engineering and [‡]Department of Chemistry, Shiv Nadar University, Dadri 201314, Uttar Pradesh, India
[§]Department of Chemistry, Miranda House, Delhi University, New Delhi 110007, India

Supporting Information

**ABSTRACT:** In this work, we report the synthesis of hydrophilic and surface-functionalized superparamagnetic iron oxide nanoparticles (SPIOs) to utilize them as nanomedicines for treating liver cancer via magnetic fluid hyperthermia (MFH)-based thermotherapy. For this purpose, initially, we have synthesized the SPIOs through coprecipitation/thermolysis methods, followed by in situ surface functionalization with short-chained molecules, such as 1,4-diaminobenzene (14DAB), 4-aminobenzoic acid (4ABA) and 3,4-diaminobenzoic acid (34DABA) and their combination with terephthalic acid (TA)/2-aminoterephthalic acid (ATA)/trimesic acid (TMA)/pyromellitic acid (PMA) molecules. The as-prepared SPIOs are investigated for their structure, morphology, water dispersibility, and magnetic properties. The heating efficacies of the SPIOs are studied in calorimetric MFH (C-MFH) with respect to their concentrations, surface coatings, dispersion medium, and applied alternating magnetic fields (AMFs). Although all of the as-prepared SPIOs have exhibited superparamagnetic behavior, only 14DAB-, 4ABA-, 34DABA-, and 4ABA-TA-coated SPIOs have shown higher magnetization values ($M_s$ = 55−71 emu $g^{-1}$) and good water dispersibility. In C-MFH studies, 34DABA-coated SPIO-based aqueous ferrofluid (AFF) has revealed faster thermal response to the applied AMF and reached therapeutic temperature even at the lowest concentration (0.5 mg $mL^{-1}$) compared with 14DAB-, 4ABA-, and 4ABA-TA-coated SPIO-based AFFs. Moreover, 34DABA-coated SPIO-based AFF has exhibited high heating efficacies (i.e., specific absorption rate/intrinsic loss power values of 432.1 W $g_{Fe}^{-1}$/5.2 $nHm^2$ $kg^{-1}$ at 0.5 mg $mL^{-1}$), which could be mainly due to (i) enhanced $\pi-\pi$ conjugation paths of surface-attached 34DABA coating molecules because of intrafunctional group attractions and (ii) improved anisotropy from the formation of clusters/linear chains of the SPIOs in ferrofluid suspensions, owing to interfunctional group attractions/interparticle interactions. Moreover, the 34DABA-coated SPIOs have demonstrated (i) very good cytocompatibility for 24/48 h incubation periods and (ii) higher killing efficiency of 61−88% (via MFH) in HepG2 liver cancer cells as compared to their treatment with only AMF/water-bath-based thermotherapy. In summary, the 34DABA-coated SPIOs are very promising heat-inducing agents for MFH-based thermotherapy and thus could be used as effective nanomedicines for cancer treatments.

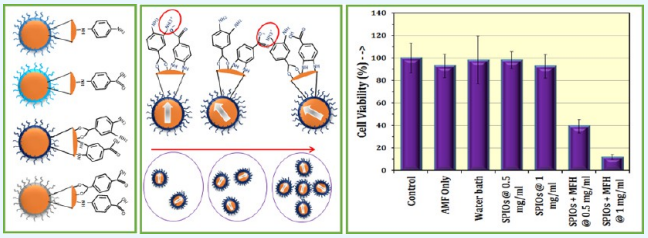


## 1. INTRODUCTION

Cancer is one of the dreadful diseases that claimed many lives worldwide. Among different clinical therapies (including radiotherapy, chemotherapy, and photothermal therapy), magnetic fluid hyperthermia (MFH)-based thermotherapy has garnered major attention in the treatment of cancer, wherein superparamagnetic iron oxide nanoparticles (SPIOs, in particular magnetite/maghemite, $Fe_3O_4/Fe_2O_3$) are primarily used to induce localized therapeutic heat (42−45 °C) inside the malignant tumors.[1−3] SPIOs are single-domain nanoparticles with superparamagnetic size (<20 nm)[4,5] and extensively studied for MFH-based cancer thermotherapy in the form of ferrofluids (FFs) by dispersing them in a carrier liquid (for e.g., water/biological media).[6−8] SPIOs are usually coated with different surface coating molecules, such as citrates, dextran, chitosan, sugars, silica, and polymers, to attain good dispersibility in the carrier liquid by inhibiting their agglomerations due to (i) the magnetic/interparticle attractions and (ii) the interactions between the surface of the SPIOs and the surrounding liquid media.[9−11] However, these long-chained surface coating molecules subsequently modify (i) physicochemical properties (size, shape, and/or crystallinity), (ii) magnetic properties (saturation magnetization, $M_s$), (iii) water dispersibility (hydrodynamic size and/or $\zeta$-potential), and (iv) biocompatibility of the SPIOs. Recently, many researchers investigated the alteration in the heating efficiencies of the SPIOs (in terms of specific absorption rate, SAR (W $g_{Fe}^{-1}$)/intrinsic loss power, ILP ($nHm^2$ $kg^{-1}$)) with respect to their physicochemical/magnetic/disper-

Received: February 3, 2018
Accepted: March 29, 2018
Published: April 10, 2018






DOI: 10.1021/acsomega.8b00207
ACS Omega 2018, 3, 3991−4005

**Scheme 1. (A) Molecular Structures of the Surface Coatings;[a] (B) Schematic Diagram for the Synthesis of the SPIOs Using Single/Dual Surfactant(s) via Co-precipitation and Thermolysis Processes; (C) Different Types of Interactions in 34DABA-Coated SPIO-Based FFs[b]**

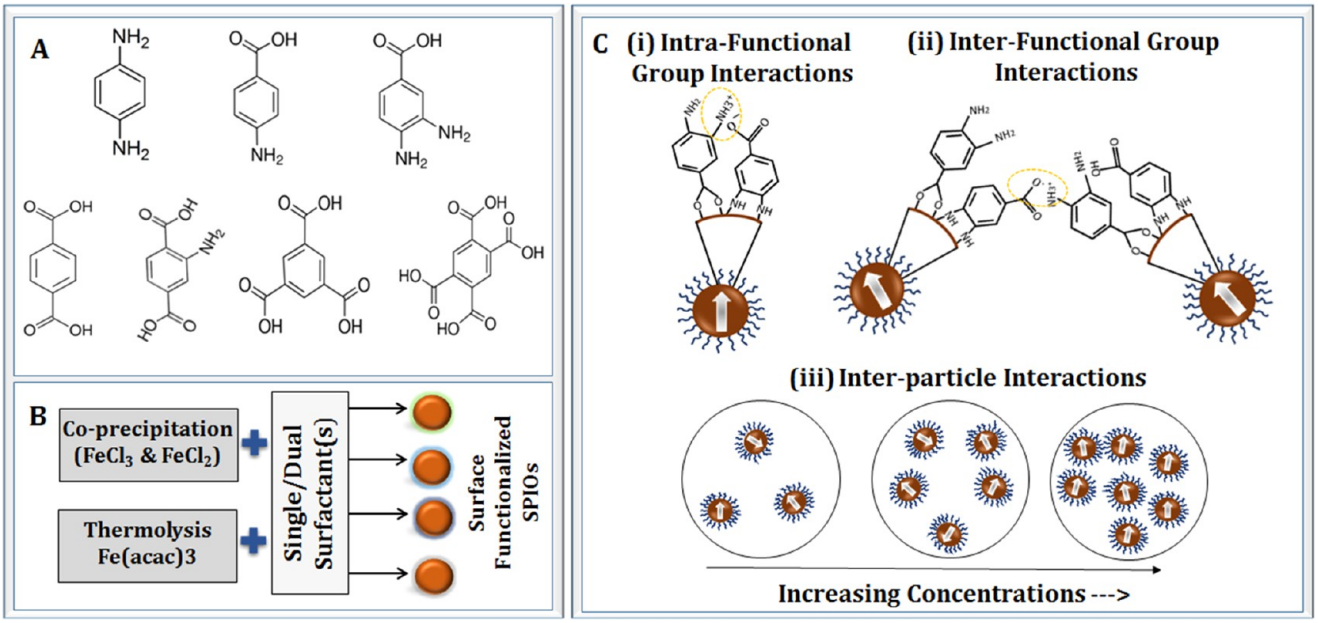


[a](i) 1,4-Diaminobenzene (14DAB), (ii) 4-aminobenzoic acid (4ABA), (iii) 3,4-diaminobenzoic acid (34DABA), (iv) terephthalic acid (TA), (v) aminoterephthalic acid (ATA), (vi) trimesic acid (TMA), and (vii) pyromellitic acid (PMA). [b](i) Intrafunctional group interactions, (ii) interfunctional group interactions, and (iii) interparticle interactions.

sibility/biocompatibility properties.[12−17] However, very less care is given to investigate the influence of the factors, including concentrations, surface coatings, applied alternating magnetic fields (AMFs with specific amplitudes ($H$) and frequencies ($f$)), and dispersion media, for improving the heating efficiency of the SPIOs in MFH studies. Moreover, the SPIO-based ferrofluids have been utilized at very high concentrations to investigate their heating efficiencies, which make them unsuitable for subsequent MFH-based cancer thermotherapies. Therefore, there is a need for synthesizing in situ functionalized SPIOs (with suitable short-chained molecules) to attain better water dispersibility, biocompatibility, and high magnetic saturation for achieving enhanced heating efficacies at their lower concentrations in appropriate AMFs ($H \times f$—near to Hergt's biological-safety limit).

Previously, we have reported the synthesis of hydrophilic SPIOs in situ functionalized with short-chained surface coating molecules (with minimum of two carboxyl functional groups), such as terephthalic acid (TA), aminoterephthalic acid (ATA), trimesic acid (TMA), and pyromellitic acid (PMA), followed by the investigation of their heating efficacy under applied AMFs.[18,19] In this work, for the first time, we report the synthesis of hydrophilic SPIOs in situ functionalized with short-chained surface coating molecules (with one or more amine functional groups), such as 1,4-diaminobenzene (14DAB), 4-aminobenzoic acid (4ABA), and 3,4-diaminobenzoic acid (34DABA), and their combination with the TA/ATA/TMA/PMA molecules via co-precipitation/thermolysis methods. These surface coating molecules are chosen because they have (i) $\pi-\pi$ conjugations to enhance the saturation magnetization of the SPIO core and magnetic response to the AMF for improving their heating efficacies and (ii) amine/carboxyl functional groups for providing them good water dispersibility in a carrier liquid medium and for further bio-/chemical-conjugations. The as-synthesized SPIOs are characterized to investigate their magnetic/physicochemical/water-dispersibility properties. The heating efficiencies of the SPIOs (in terms of SAR/ILP values) influenced by the fundamental parameters, including surface coatings, concentrations, applied AMFs (with $H \times f$ values of 2.4−9.9 $GAm^{-1}$ $s^{-1}$), and dispersion media of their ferrofluid suspension are explored via calorimetric MFH (C-MFH) studies. Moreover, the selected SPIOs (with enhanced saturation magnetization, water dispersibility, and SAR/ILP values) are further studied for in vitro MFH-based thermotherapy for the treatment of liver (HepG2) cancer and compared with the water-bath based conventional thermotherapy (WCTT, without SPIOs).

## 2. MATERIALS AND METHODS

**2.1. Materials.** Terephthalic acid (TA), 2-aminoterephthalic acid (ATA), 3,4-diaminobenzoic acid (34DABA), iron (III) acetylacetonate, iron (II) chloride, potassium hexacyanoferrate, iron (III) chloride, and trypan blue are procured from Sigma-Aldrich. Trimesic acid (TMA), 4-aminobenzoic acid (4ABA), and pyromellitic acid (PMA) are obtained from Alfa Aeser. 1,4-Diaminobenzene (14DAB) is obtained from CDH chemicals. Ammonium persulfate (APS), potassium thiocyanate (KSCN), triethylene glycol (TEG), $NH_4OH$, diethylene glycol (DEG), glycerol (GC), ethylene glycol (EG), HCl (37%), and ethanol are obtained from Fisher Scientific. Phosphate buffer saline (PBS), fetal bovine serum (FBS), and Dulbecco's modified eagle medium (DMEM) are purchased from Gibco Life technologies.

**2.2. Synthesis Methods.** SPIOs are synthesized via chemical co-precipitation and thermolysis methods, as reported elsewhere, with some minor modifications.[19] The SPIOs are in situ surface functionalized by using individual 14DAB, 4ABA, and 34DABA molecules (i.e., single surfactant) and their combination with TA/ATA/TMA/PMA molecules (i.e., dual



DOI: 10.1021/acsomega.8b00207
ACS Omega 2018, 3, 3991−4005

surfactants). Scheme 1A,B represents the surface coating molecules (i.e., 14DAB, 4ABA, 34DABA, TA, ATA, TMA, and PMA) and chemical synthesis of surface-functionalized SPIOs, respectively.

*2.2.1. Co-precipitation Method.* Briefly, to synthesize single-surfactant-coated SPIOs, iron (III) and (II) chlorides in a 2:1 molar ratio and appropriate amount of 14DAB or 4ABA or 34DABA are mixed in Millipore water. The mixture solution is heated to 80 °C and magnetically stirred for 60 min under nitrogen ($N_2$) atmosphere. Then, $NH_4OH$ is added to the mixture solution and vigorously stirred for another 60 min at the same temperature. Thereafter, the resultant solution is cooled to room temperature by removing the heat source. At last, the precipitated nanoparticles are magnetically separated and then washed with 1:1 (v/v) mixture of Millipore water and ethanol. Moreover, the dual surfactant-coated SPIOs are prepared in a similar fashion by using 14DAB/4ABA/34DABA molecules combined with TA/ATA/TMA/PMA molecules in an equal molar ratio.

*2.2.2. Thermolysis Method.* Briefly, to synthesize single-surfactant-coated SPIOs, iron (III) acetylacetonate and 14DAB or 4ABA or 34DABA molecules are dissolved in TEG and the mixture solution is dehydrated at 120 °C for 60 min under $N_2$ atmosphere. Then, the mixture solution is further heated to a specific refluxing temperature (refer Table S1) and maintained for another 60 min. Thereafter, the resultant mixture solution is brought down to room temperature by removing the heat source. At last, the precipitated nanoparticles are magnetically separated and then washed with 1:1 (v/v) mixture of Millipore water and ethanol. Moreover, the dual surfactant-coated SPIOs are prepared in a similar manner by using 14DAB/4ABA/34DABA molecules combined with TA/ATA/TMA/PMA molecules in an equal molar ratio.

*2.2.3. SPIO Samples.* The sample details along with the reaction conditions, including the temperature, time, and the surfactant(s) (single/dual category) for co-precipitation and thermolysis methods are given in Table S1. The SPIOs S1, S2, S11, and S12 are formed using the single surfactant, i.e., 14DAB and 4ABA molecules via both the co-precipitation and thermolysis methods, whereas the SPIO S3 is formed only via co-precipitation but not by the thermolysis method using the single surfactant, i.e., 34DABA molecules. The SPIOs S4, S5, S8, S9, S13, S14, S15, and S16 are also formed using 14DAB-TA, 14DAB-ATA, 4ABA-TA, and 4ABA-ATA dual surfactants through both the co-precipitation and thermolysis methods. However, the SPIOs S6, S7, and S10 are formed using 14DAB-TMA, 14DAB-PMA, and 4ABA-PMA dual surfactants only via co-precipitation but not by the thermolysis method. Moreover, the SPIOs are not formed using 34DABA-TA, 34DABA-ATA, 34DABA-TMA, and 34DABA-PMA dual surfactants via both the co-precipitation and thermolysis methods.

*2.2.4. Ferrofluid (FF) Samples.* Aqueous ferrofluids (AFFs) are prepared by dispersing the as-synthesized single/dual surfactant(s)-coated SPIOs in a definite volume of aqueous medium, and the iron (Fe) concentrations are determined via UV−vis spectrophotometry. Briefly, the AFFs are digested with HCl at 80 °C for 2 h after proper dilution. Then, the resultant solution is mixed with APS and KSCN (0.1 M) to form a red-colored iron−thiocyanate complex, whose absorbance is measured at 474 nm to determine the Fe concentration with reference to a standard curve. Thereafter, AFFs are diluted with water to obtain the concentrations of 0.5, 1, 2, 4, and 8 $mg_{Fe}$ $mL^{-1}$ (hereafter marked as mg $mL^{-1}$) accordingly.

To prepare the FFs in other media, appropriate amount of AFFs are taken in a vial and then the SPIOs are magnetically separated completely from the aqueous medium and subsequently dispersed in a definite volume of (i) nonbiological media, EG, DEG, TEG, and GC, and (ii) biological media, PBS, DMEM, DMEM + 5% FBS, and FBS, through a vigorous vortexing process to provide nonbiological FFs (NBFFs) and biological FFs (BFFs), respectively.

**2.3. Materials Characterization.** As-prepared SPIOs are initially characterized via a thermogravimetric analyzer (TGA, SII 6300 EXSTAR) in a temperature range of 30−800 °C and a vibrating sample magnetometer (VSM, PAR 155) at room temperature to investigate their amount of surface coatings and magnetic properties, respectively. The selected SPIOs (on the basis of the TGA/VSM results) are further characterized by using a Fourier transform infrared spectrometer (FTIR, ThermoFisher Scientific Nicolet iS 5, by following the potassium bromide (KBr) pellet method), transmission electron microscope (TEM, Technai G2 20 S-TWIN, operated at 200 kV), and X-ray diffraction (XRD, Bruker D8 Advance—Cu K$\alpha$ ($\lambda$ = 1.54 nm) with a scan range ($2\theta$) of 20−80°) to identify their structure (in terms of attached surface coating molecules and phase purity) and morphology (i.e., size and shape). Moreover, the hydrodynamic diameters and $\zeta$-potentials of the selected SPIOs are determined via the dynamic light scattering (DLS, Horiba nanoPartica SZ-100-Z, equipped with a 532 nm laser) technique by considering the average of three readings.

**2.4. Calorimetric MFH Studies.** The heating profiles of the SPIOs in the form of AFFs are investigated via calorimetric MFH (C-MFH) studies by using a magnetic hyperthermia instrument (magneTherm-nanoTherics).[20] Briefly, 1 mL of the AFFs with concentrations of 0.5−8 mg $mL^{-1}$ is taken in a sample vial, which is enclosed in a Styrofoam-based container and kept inside the induction coils (which is sustained at ∼37 °C via a water recirculating chiller) of the hyperthermia instrument. The initial temperature of AFFs is observed using an optical probe for 120 s to ensure that the temperature from the coils does not induce any heat on the ferrofluids. Then, the AFFs are subjected to AMFs at specific amplitudes ($H$ = 7−18 kA $m^{-1}$) and frequencies ($f$ = 175−1001 kHz). Subsequently, the time-dependent temperature (TDT) rise of the AFFs is determined till the temperature reaches a fixed temperature (45 °C) or maximum temperature (≤45 °C) within 30 min (1800 s). Then, the heating efficiencies of AFFs are calculated in terms of SAR, considering the initial slopes of TDT curves as per the following equation

$$\mathrm{SAR} = \frac{C_{\mathrm{samp}} \times \rho_{\mathrm{samp}}}{m\mathrm{Fe}} \frac{\Delta T}{\Delta t} \tag{1}$$

where $C_{\mathrm{samp}}$ and $\rho_{\mathrm{samp}}$ are the specific heat capacity and density of the dispersion medium of AFF, respectively, $m$Fe is the mass fraction of Fe (in grams) in FFs, and $\Delta T/\Delta t$ is the initial slope from TDT curve. Similarly, the TDT rise experiments are performed for NBFFs and BFFs and the corresponding SAR values are calculated. Moreover, intrinsic loss power (ILP, $nHm^2$ $kg^{-1}$, based on normalized SAR) values are also calculated for the AFFs/NBFFs/BFFs as per the following equation

$$\mathrm{ILP} = \frac{\mathrm{SAR}}{H^2 f} \tag{2}$$

**2.5. Biological Studies.** *2.5.1. In Vitro Cell Viability.* In vitro cell viability of the selected SPIOs is determined in liver (HepG2) cancer cells via trypan blue assay at two different time



DOI: 10.1021/acsomega.8b00207
ACS Omega 2018, 3, 3991−4005

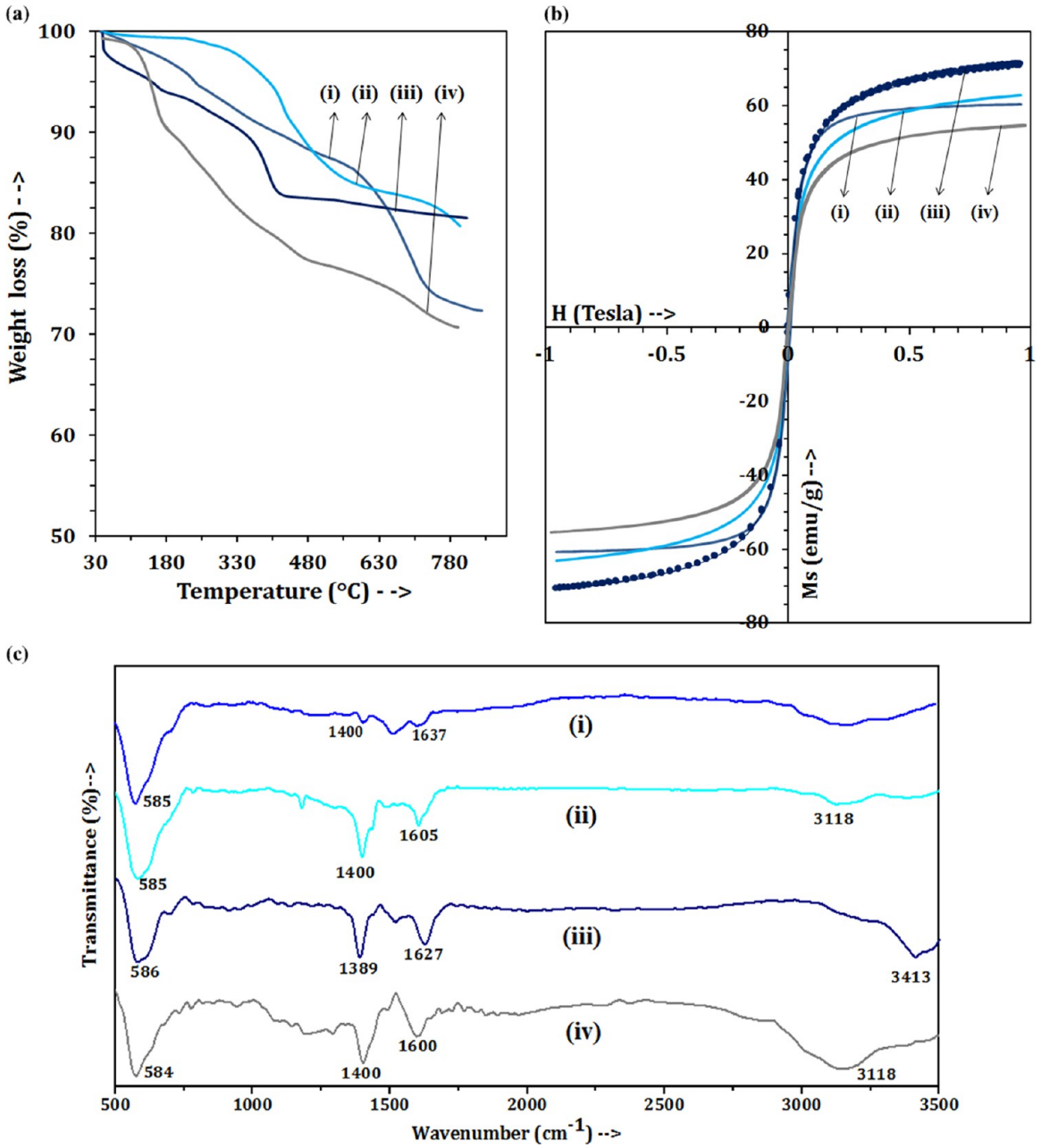


**Figure 1.** (A) TGA curves of the SPIOs: (i) S1 (14DAB-coated), (ii) S2 (4ABA-coated), (iii) S3 (34DABA-coated), and (iv) S8 (4ABA-TA-coated). (B) VSM curves of the SPIOs: (i) S1 (14DAB-coated), (ii) S2 (4ABA-coated), (iii) S3 (34DABA-coated), and (iv) S8 (4ABA-TA-coated). (C) FTIR spectra of the SPIOs: (i) S1 (14DAB-coated), (ii) S2 (4ABA-coated), (iii) S3 (34DABA-coated), and (iv) S8 (4ABA-TA-coated).

periods (24 and 48 h) on the basis of the standard protocol, as reported elsewhere, with minor modifications.[21,22] At the beginning, HepG2 cancer cells are seeded in 24-well plates with a density of ∼35 000 cells per well and incubated for 24 h. Then, the SPIOs at specific concentrations (5, 10, 15, 20, and 25 $\mu g_{Fe}$) per well are incubated in triplicates at 37 °C under 5% $CO_2$. After 24/48 h incubation period, the cancer cells are washed with PBS twice and optical microscopic images (Leica DMi1 inverted microscope) are taken to confirm the presence of the SPIOs. Later, the cells are detached by using trypsin and then small aliquots of HepG2 cancer cells are mixed with an equal volume of 0.4% trypan blue. Finally, the number of live and dead cells is counted via a hemocytometer (Neubauer Chamber, Gem instruments) and the cell viability is calculated ($n$ = 3) by using the following formula

$$\text{cell viability (in \%)} = \frac{100 \times \text{no. of unstained cells}}{\text{no. of unstained and stained cells}} \quad (3)$$

where the unstained cells indicate the live cells and the stained cells indicate the dead cells due to the exposure of cellular components to the trypan blue dye.

*2.5.2. In Vitro MFH and WCTT.* In vitro MFH studies are performed as reported elsewhere, with some minor alterations.[21,23,24] Herein, 1 × $10^6$ liver (HepG2) cancer cells in DMEM medium (with 10% FBS) are centrifuged to obtain a pellet, which is resuspended in media containing the selected SPIOs at two different concentrations, i.e., 0.5 and 1 mg $mL^{-1}$. Then, they are subjected to AMF (with an amplitude of 10.9 kA $m^{-1}$ at a frequency of 751.51 kHz) to reach the therapeutic



DOI: 10.1021/acsomega.8b00207
ACS Omega 2018, 3, 3991−4005

**Table 1. Surface Coatings, TGA Secondary Weight Loss (%), Saturation Magnetization ($M_s$, emu $g^{-1}$), TEM Size (nm), Mean Hydrodynamic Diameter ($D_h$, nm), and ζ-Potential (ζ, mV) of the SPIOs (S1, S2, S3, and S8) Synthesized via a Chemical Co-precipitation Process**

| sample code (SPIOs/FFs) | surface coatings | TGA secondary weight loss (approx. in %) | saturation magnetization ($M_s$, emu $g^{-1}$) | TEM size (nm) | mean hydrodynamic diameter ($D_h$, nm) | mean ζ-potential (ζ, mV) |
|---|---|---|---|---|---|---|
| S1/AFF-1 | 14DAB | 17.2 | 60.4 | 6 ± 2 | 163.3 | −31 |
| S2/AFF-2 | 4ABA | 15.3 | 62.8 | 8 ± 2 | 137.1 | −43 |
| S3/AFF-3 | 34DABA | 12.0 | 71.3 | 10 ± 3 | 193.5 | −33 |
| S8/AFF-4 | 4ABA-TA | 18.8 | 54.5 | 8 ± 3 | 149.3 | −31 |

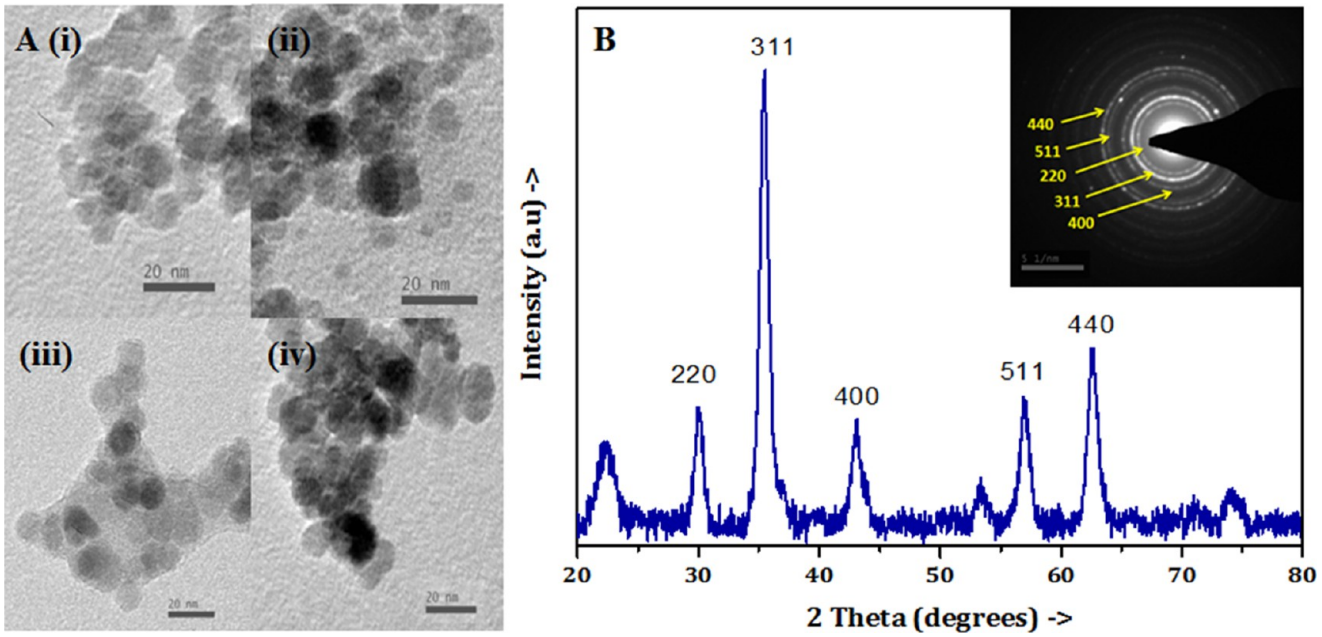


**Figure 2.** (A) TEM images of the SPIOs: (i) S1 (14DAB-coated), (ii) S2 (4ABA-coated), (iii) S3 (34DABA-coated), and (iv) S8 (4ABA-TA-coated). (B) XRD pattern of the 34DABA-coated SPIOs (S3), where the inset represents the SAED pattern of the 34DABA-coated SPIOs (S3).

temperature (42 °C), which is then maintained for the next 60 min by attuning the AMF. In addition, the equal number of liver cancer cells is (i) treated under same AMF (without SPIOs) and (ii) incubated with only SPIOs (without AMF) at 0.5 and 1 mg $mL^{-1}$ concentration. After MFH treatment, ∼40 μL of cell suspension (equivalent to ∼40 000 cells) is mixed with appropriate media and plated in triplicates, followed by 72 h of incubation at 37 °C under 5% $CO_2$. A similar procedure is followed for the cells treated with only AMF and only SPIOs at 0.5 and 1 mg $mL^{-1}$ concentrations. Finally, the trypan blue assay is performed to determine the viability of cancer cells after washing the wells with PBS twice, where microscopic images are taken after the washing process.

Moreover, in vitro water-bath-based conventional thermotherapy (WCTT) is performed as reported elsewhere, with some minor modifications.[25] Briefly, $1 \times 10^6$ HepG2 cancer cells (in a vial) are subjected to therapeutic heat at 42 °C. Herein, a recirculating chiller (Grant Instruments, U.K.) is used to reach the therapeutic temperature (42 °C) in the cell suspension (from the initial temperature of 30 °C) and maintained for 60 min. Moreover, the vial is taken out every 15 min and slightly tapped for 5 s to make a uniform suspension and further involved in WCTT. Later, ∼40 μL of cell suspension is taken, resuspended in media, plated in triplicates in a 24-well plate, and then incubated for 72 h. Finally, the viability of the cancer cells is determined via the trypan blue assay after washing the wells with PBS twice, where microscopic images are taken after the washing process. The cells without AMF/SPIOs/SPIOs + MFH/WCTT are used as a control.

*2.5.3. In Vitro Cellular Uptake.* Intracellular uptake of the SPIOs is qualitatively determined during (i) cytotoxicity and (ii) MFH experiments via the Prussian blue staining method, as reported elsewhere, with minor modifications.[26] At first, similar to the cytotoxicity experiments, the SPIOs at 15 $\mu g_{Fe}$ concentration are incubated with cancer cells (having initial density of ∼35 000 cells per well) in triplicates for 24/48 h. After the incubation period, the cells are fixed with 4% formaldehyde for 20 min and then incubated for another 20 min with a mixture solution of HCl and potassium hexacyanoferrate (each 4%). Finally, the wells are washed with PBS twice and then the microscopic images are taken to confirm the in vitro uptake of SPIOs by the cancer cells. In a similar fashion, after the MFH treatment, the cancer cells with/without SPIOs/SPIOs + MFH are incubated for 72 h, then dyed with Prussian blue as mentioned above and finally the microscopic images are taken after washing with PBS twice.

## 3. RESULTS AND DISCUSSION

**3.1. Surface Coatings and Magnetic Properties.** Initially, surface coatings and magnetic properties of all of the as-prepared SPIOs (via co-precipitation and thermolysis methods) are characterized through TGA and VSM.

*3.1.1. TGA.* Figures 1A(i–iv), S1A(i–vi), and S1B(i–vi) show the TGA curves of all of the SPIO samples (S1–S16). The TGA



DOI: 10.1021/acsomega.8b00207
ACS Omega 2018, 3, 3991−4005

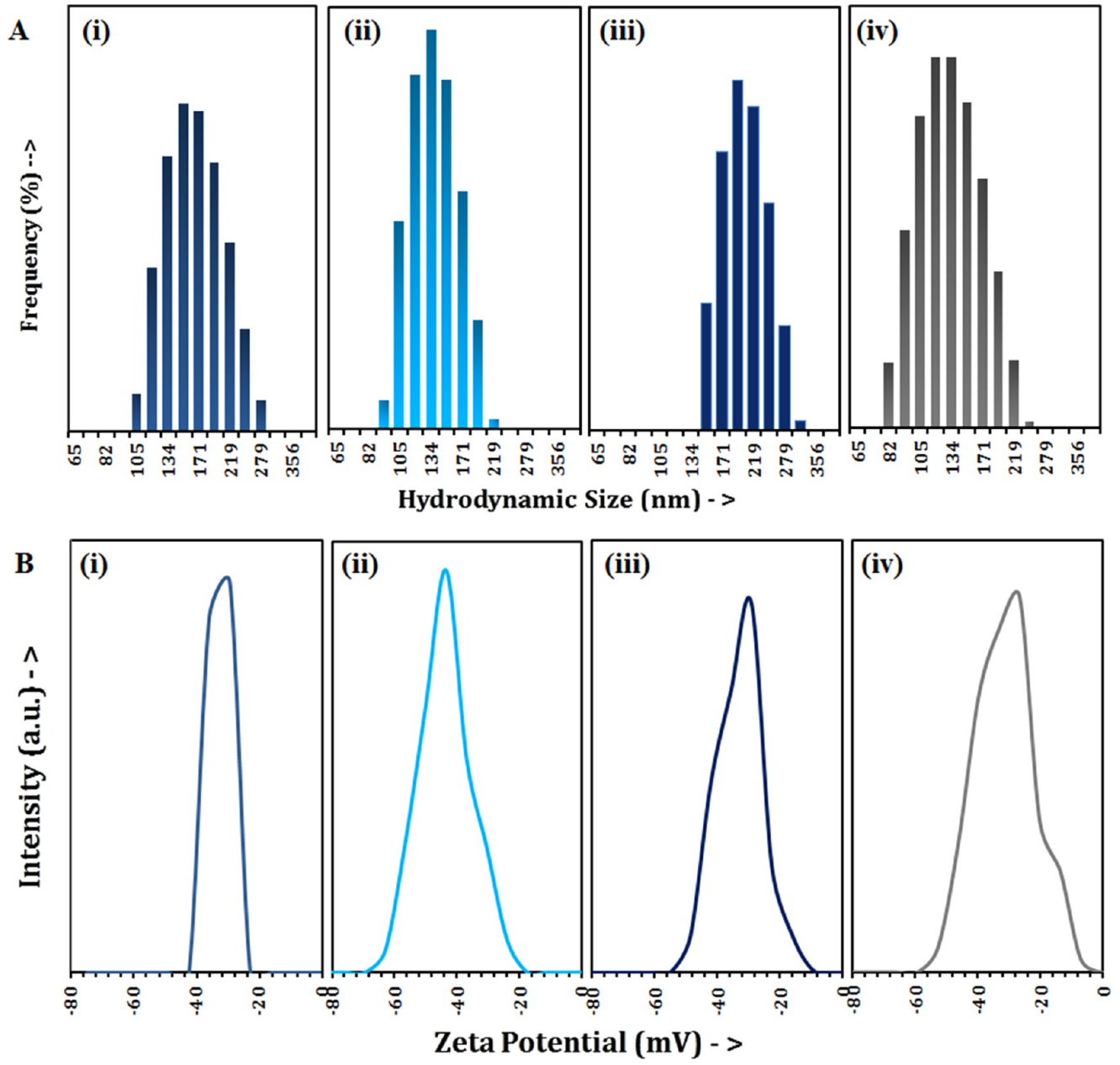


**Figure 3.** (A) Hydrodynamic size distribution plots of the SPIOs: (i) S1 (14DAB-coated), (ii) S2 (4ABA-coated), (iii) S3 (34DABA-coated), and (iv) S8 (4ABA-TA-coated). (B) ζ-Potential plots of the SPIOs: (i) S1 (14DAB-coated), (ii) S2 (4ABA-coated), (iii) S3 (34DABA-coated), and (iv) S8 (4ABA-TA-coated).

curves show two weight losses: (i) primary loss in the temperature range of 30−200 °C and (ii) secondary loss in the temperature range of 200−800 °C due to the decomposition of physically adsorbed water molecules and chemically adsorbed surface coatings, respectively. The corresponding amounts of the single/dual surfactant(s) attached to the surface of the SPIOs are given in Table S2. It can be seen that the amount of surface coatings are comparably lower for the single surfactant-coated SPIOs (S1−S3 and S11−S12) than the dual surfactant-coated SPIOs (S4−S10 and S13−S16) synthesized via co-precipitation and thermolysis methods.

*3.1.2. VSM.* Figures 1B(i−iv), S2A(i−vi), and S2B(i−vi) show the magnetization ($M$−$H$) curves of all of the SPIOs (S1−S16) at room temperature, and the corresponding magnetization ($M_s$) values are given in Table S2. Zero coercivity and zero remanence of the $M$−$H$ curves confirm the superparamagnetic behavior of all of the SPIOs.[27]

In the co-precipitation process, S1, S2, and S3 (i.e., the SPIOs coated with single surfactant, 14DAB, 4ABA, and 34DABA, molecules) have shown respective $M_s$ values of 60.4, 62.8, and 71.3 emu $g^{-1}$. On the other hand, S4, S5, S6, S7, S8, S9, and S10 (i.e., the SPIOs coated with dual surfactants, 14DAB-TA, 14DAB-ATA, 14DAB-TMA, 14DAB-PMA, 4ABA-TA, 4ABA-ATA, and 4ABA-PMA molecules) have shown the $M_s$ values of 16.8, 21.3, 21.9, 15.2, 54.5, 16.7, and 46.2 emu $g^{-1}$, respectively.

Similarly, in the thermolysis process, S11 and S12 (i.e., the SPIOs coated with single surfactants, 14DAB and 4ABA molecules) have shown respective $M_s$ values of 40.8 and 46.8 emu $g^{-1}$, respectively. On the other hand, S13, S14, S15, and S16 (i.e., the SPIOs coated with dual surfactants, 14DAB-TA,



DOI: 10.1021/acsomega.8b00207
*ACS Omega* 2018, 3, 3991−4005

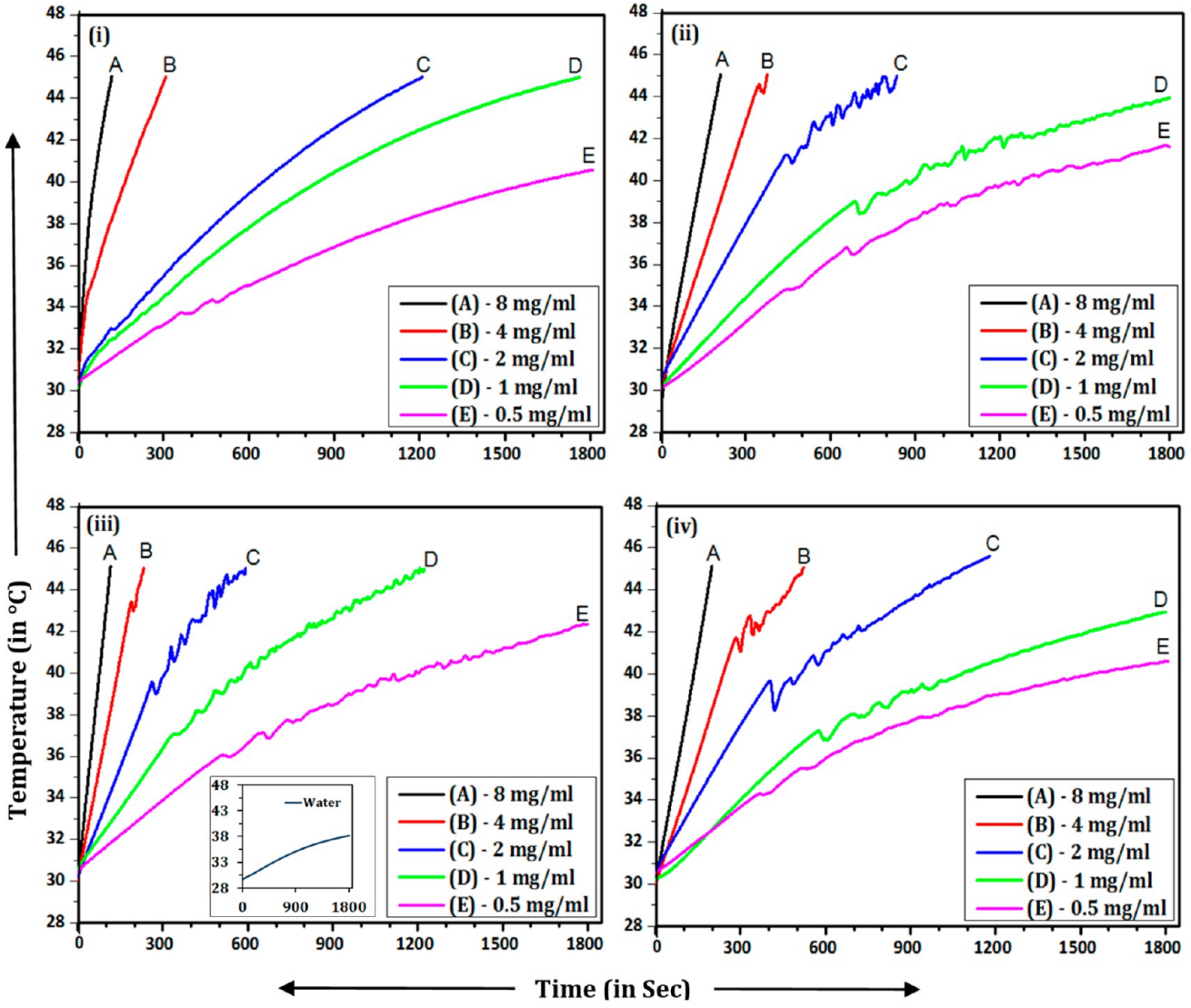


**Figure 4.** Time-dependent temperature (TDT) curve of 1 mL AFFs with concentrations of (A) 8, (B) 4, (C) 2, (D) 1, and (E) 0.5 mg $mL^{-1}$ on exposure to AMF with $H \times f$ value of 8.2 $GAm^{-1}$ $s^{-1}$: (i) AFF-1 (14DAB-coated SPIOs), (ii) AFF-2 (4ABA-coated SPIOs), (iii) AFF-3 (34DABA-coated SPIOs), and (iv) AFF-4 (4ABA-TA-coated SPIOs). Inset in (iii) represents the TDT curve of water (without SPIOs) on exposure to AMF with an $H \times f$ value of 8.2 $GAm^{-1}$ $s^{-1}$.

14DAB-ATA, 4ABA-TA, and 4ABA-ATA molecules) have shown the $M_s$ values of 5.5, 7.2, 44.9, and 24.4 emu $g^{-1}$, respectively.

It can be seen that dual-surfactant-coated SPIOs (S4−S7, S9, S10, S13, S14, and S16) have shown lower $M_s$ values than the single-surfactant-coated SPIOs (S1−S3 and S11−S12) due to large amounts of surface coating for the dual-surfactant-coated SPIOs except 4ABA-TA-coated SPIOs (S8 and S15) that have shown slightly higher $M_s$ values due to the small amount of surface coatings (as confirmed by the TGA results). The highest $M_s$ value of 71.3 emu $g^{-1}$ is attained for the 34DABA-coated SPIOs (S3) due to the lowest amount of surface coatings, as confirmed by the TGA as well.

Thus, on the basis of the TGA/VSM results, the S1, S2, S3, and S8 (refer Table 1) are selected for further characterizations due to their lower amount of surface coatings that correspond to their higher saturation magnetization ($M_s$) values, i.e., above 50 emu $g^{-1}$, which is essential to attain enhanced heating effects in MFH studies.[18]

**3.2. Structure, Morphology, and Dispersibility.** The selected SPIOs (S1, S2, S3, and S8) are characterized by FTIR, TEM, XRD, and DLS to investigate their structure, morphology, and dispersibility in the carrier liquid.

*3.2.1. FTIR.* Figure 1C(i−iv) depicts the FTIR spectra of 14DAB-, 4ABA-, 34DABA-, and 4ABA-TA coated SPIOs (i.e., S1, S2, S3, and S8), respectively. The absorption peaks of 584−586 $cm^{-1}$ correspond to the Fe−O stretching vibrations of the iron oxide core in each of the SPIOs, and the absorption peaks beyond 600 $cm^{-1}$ are ascribed to the vibrations from the coatings adsorbed to the surface of the SPIOs. The absorption peaks at the region of 1390−1600 $cm^{-1}$ are assigned to the symmetric/asymmetric vibrations of the amino groups of 14DAB, 4ABA, and 34DABA molecules attached to the surface of the SPIOs. Moreover, the broad absorption peaks at 3100−3400 $cm^{-1}$ in Figure 1C(ii−iv) correspond to the O−H bonds of the carboxylic functional groups of 4ABA, 34DABA, and TA molecules attached to the respective SPIOs. Thus, the presence of 14DAB, 4ABA, 34DABA, and 4ABA-TA coating molecules attached to the surface of the SPIOs is confirmed.



DOI: 10.1021/acsomega.8b00207
ACS Omega 2018, 3, 3991−4005

Table 2. SAR (W $g_{Fe}^{-1}$) and ILP ($nHm^2\ kg^{-1}$) Values of the 34DABA-Coated SPIOs Dispersed in Aqueous Medium (AFF-3)

| | | | | | SAR (W $g_{Fe}^{-1}$) | | | | | ILP ($nHm^2\ kg^{-1}$) | | | | |
|---|---|---|---|---|---|---|---|---|---|---|---|---|---|---|
| $f$ (kHz) | $H$ (kA $m^{-1}$) | $H \times f$ ($GAm^{-1}s^{-1}$) | Hergt's limit ($H \times f$, $GAm^{-1}s^{-1}$) | ratio of $H \times f$ of this work to Hergt's limit | 0.5 (mg $mL^{-1}$) | 1 (mg $mL^{-1}$) | 2 (mg $mL^{-1}$) | 4 (mg $mL^{-1}$) | 8 (mg $mL^{-1}$) | 0.5 (mg $mL^{-1}$) | 1 (mg $mL^{-1}$) | 2 (mg $mL^{-1}$) | 4 (mg $mL^{-1}$) | 8 (mg $mL^{-1}$) |
| 175.2 | 13.90 | 2.44 | 5.00 | 0.49 | 48.6 | 36.8 | 26.2 | 21.6 | 21.4 | 1.4 | 1.1 | 0.8 | 0.6 | 0.6 |
| 262.2 | 13.80 | 3.61 | | 0.72 | 100.5 | 70.8 | 44.8 | 36.1 | 31.1 | 2.0 | 1.4 | 0.9 | 0.7 | 0.6 |
| 330.3 | 10.39 | 3.43 | | 0.69 | 82.1 | 62.0 | 47.9 | 37.2 | 32.1 | 2.3 | 1.7 | 1.3 | 1.0 | 0.9 |
| 474.7 | 8.66 | 4.11 | | 0.82 | 140.7 | 82.1 | 54.2 | 42.5 | 32.9 | 4.0 | 2.3 | 1.5 | 1.2 | 0.9 |
| 522.2 | 15.39 | 8.03 | | 1.61 | 189.3 | 98.8 | 67.6 | 60.3 | 46.1 | 1.5 | 0.8 | 0.5 | 0.5 | 0.4 |
| 632.3 | 7.10 | 4.48 | | 0.90 | 165.8 | 81.2 | 51.7 | 37.1 | 32.3 | 5.2 | 2.6 | 1.6 | 1.2 | 1.0 |
| 751.5 | 10.95 | 8.22 | | 1.64 | 330.8 | 207.3 | 84.2 | 79.8 | 77.9 | 3.7 | 2.3 | 0.9 | 0.9 | 0.9 |
| 1001.1 | 9.98 | 9.99 | | 2.00 | 432.1 | 233.6 | 85.0 | 80.7 | 63.3 | 4.3 | 2.3 | 0.9 | 0.8 | 0.6 |

*3.2.2. TEM and XRD.* Figure 2A(i–iv) displays the TEM images of the 14DAB-, 4ABA-, 34DABA-, and 4ABA-TA-coated SPIOs (S1, S2, S3, and S8), respectively, where the average particle sizes are calculated via a software (Image J) by considering ∼30–40 number of nanoparticles. The average particle sizes of S1, S2, S3, and S8 are determined as 6 ± 2, 8 ± 2, 10 ± 2, and 8 ± 3 nm, respectively (refer Table 1), which indicates that the sizes of as-synthesized nanoparticles are within superparamagnetic regime (<20 nm). Moreover, the shapes of all of the SPIOs (i.e., S1–S3 and S8) are found to be spherical.

Figure 2B illustrates XRD pattern of 34DABA-coated SPIOs (S3), where the diffraction peaks, including (220), (311), (400), (511), and (440), confirm the $Fe_3O_4$ (magnetite) phase with inverse spinel structure (JCPDS file, 19-0629). Moreover, the inset in Figure 2B displays the selected area electron diffraction (SAED) pattern for S3, which also clearly shows the diffraction rings corresponding to the lattice planes of (220), (311), (400), (511), and (440) to agree with the XRD result. Similar XRD/SAED patterns can be obtained for other three samples as well. In addition, the crystallite size ($D$) for S3 is calculated to be 9.78 nm by using the Scherrer formula (which is $D = K\lambda/(\beta \cos \theta)$, where $K$ is a constant, $\lambda$ is the wavelength of X-ray, and $\beta$ is the peak width of half-maximum) on consideration of (311) diffraction peak.

*3.2.3. DLS.* Figure 3A(i–iv) depicts the hydrodynamic size ($D_h$) distribution plots of the 4DAB-, 4ABA-, 34DABA-, and 4ABA-TA-coated SPIOs (S1, S2, S3, and S8) dispersed in water-based ferrofluids (AFF-1, AFF-2, AFF-3, and AFF-4), respectively. The mean $D_h$ values are determined as 163.3, 137.1, 193.5, and 149.3 nm for the S1, S2, S3, and S8 samples, respectively (refer Table 1). It can be seen that the $D_h$ of the SPIOs is larger than their TEM sizes, which is mainly attributed to the formation of small clusters/aggregates and linear chains/loops of the SPIOs in the ferrofluid suspension due to (i) magnetic dipole–dipole/interparticle interactions and/or (ii) hydrogen bonding between the nearby surface-attached functional groups.[28] Figure 3B(i–iv) displays the $\zeta$-potential ($\zeta$) plots of the 4DAB-, 4ABA-, 34DABA-, and 4ABA-TA-coated SPIOs (S1, S2, S3, and S8) dispersed in water-based ferrofluids (AFF-1, AFF-2, AFF-3, and AFF-4), and the corresponding mean $\zeta$-potentials are determined as −31, −43, −33, and −31 mV, respectively (refer Table 1). These results confirm that the SPIOs have very good water dispersibility because generally the nanoparticles are considered to be stable in suspensions if their $\zeta$ potentials are near/above ±30 mV.[29]

Thus, on the basis of the TGA/VSM/FTIR/TEM/XRD/DLS results, 4DAB-, 4ABA-, 34DABA-, and 4ABA-TA-coated SPIOs (S1, S2, S3, and S8) dispersed in the aqueous ferrofluids (AFFs) are selected for further MFH studies.

**3.3. Calorimetric MFH.** Calorimetric MFH (C-MFH) experiments of the 4DAB-, 4ABA-, 34DABA-, and 4ABA-TA-coated SPIO (S1, S2, S3, and S8)-based AFFs (AFF-1, AFF-2, AFF-3, and AFF-4, respectively) are performed at concentrations ranging from 0.5 to 8 mg $mL^{-1}$ on exposure to the AMF with a specific amplitude and frequency. Herein, the heat generated by the SPIOs is mainly due to the following: (i) Néel relaxation mechanism (rotation of magnetic moments) and (ii) Brownian relaxation mechanism (physical rotation of the particles). The time periods taken by AFFs to reach the fixed/maximum temperature (≤45 °C) within the stipulated time of 30 min and their corresponding heating efficacies (SAR values) are given in Table S3. The effects of the fundamental parameters, including concentrations, surface coatings, applied alternating magnetic



DOI: 10.1021/acsomega.8b00207
ACS Omega 2018, 3, 3991–4005

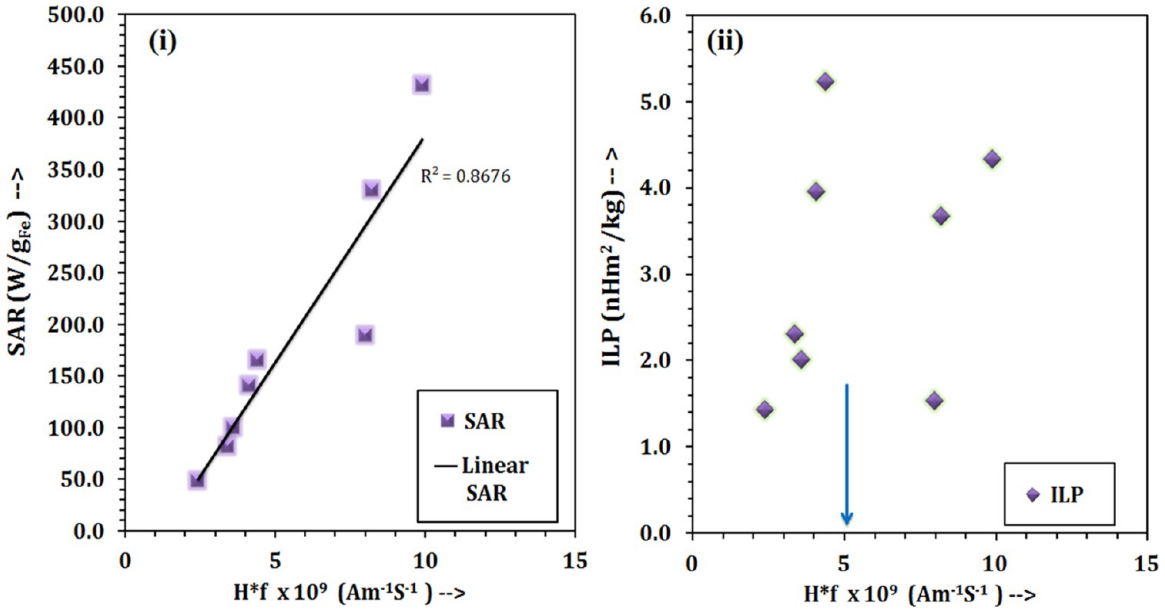


**Figure 5.** (i) SAR values vs $H \times f$ for AFF-3 (34DABA-coated SPIOs) at 0.5 mg mL$^{-1}$ concentration. (ii) ILP values vs $H \times f$ for AFF-3 (34DABA-coated SPIOs) at 0.5 mg mL$^{-1}$ concentration, where the blue line with arrow indicates Hergt's safety limit of 5 GAm$^{-1}$ s$^{-1}$.

fields (AMFs), and dispersion media, on the heating efficiencies of the SPIOs/AFFs are discussed subsequently.

*3.3.1. Effects of Concentrations and Surface Coatings.* Initially, AFFs are exposed to AMF with an amplitude ($H$) of 10.9 kA m$^{-1}$ at a frequency ($f$) of 751.5 kHz ($H \times f \sim 8.2$ GAm$^{-1}$ s$^{-1}$) to study the effects of concentrations/surface coatings on their heating efficiencies. Figure 4i–iv depicts the time-dependent temperature (TDT) curves for AFF-1–AFF-4, respectively. It can be seen that the time taken by the AFFs to reach the fixed/maximum temperature (≤45 °C) is significantly decreased with the increment in their concentrations (refer Table S3). For instance, AFF-1 has reached 45 °C in 29.3, 20.1, 5.1, and 1.9 min for 1, 2, 4, and 8 mg mL$^{-1}$ concentrations, respectively. Likewise, AFF-2 has taken 13.9, 6.2, and 3.5 min to reach 45 °C at 2, 4, and 8 mg mL$^{-1}$ concentrations, respectively. A similar trend in time reduction with the increase of concentrations to reach the fixed/maximum temperature is observed for AFF-3 and AFF-4 as well. Nevertheless, AFF-3 has taken shorter time periods as compared with AFF-1, AFF-2, and AFF-4 to reach a fixed/maximum temperature for all of the concentrations. The faster heating profile of AFF-3 could be mainly ascribed to the larger particle size (i.e., 10 nm), high saturation magnetization (i.e., 71.3 emu g$^{-1}$), and enhanced relaxations (because of the formation of comparably large clusters/aggregates of the SPIOs (S3), as evident from their DLS result) in association with higher motion/rotation (of the nanoparticles in aqueous medium) driven by the applied magnetic field.[30,31]

Moreover, AFF-3 has reached the therapeutic temperature of 42 °C at the lowest concentration (0.5 mg mL$^{-1}$) as compared with AFF-1, AFF-2, and AFF-4 (42 °C, not reached) within the stipulated time of 30 min. Furthermore, AFF-3 has shown the highest SAR (calculated as per eq 1) values (330.8 and 207.3 W $g_{Fe}^{-1}$), as compared with the SAR values of AFF-1 (302.3 and 176.6 W $g_{Fe}^{-1}$), AFF-2 (219.4 and 83.3 W $g_{Fe}^{-1}$), and AFF-4 (287.2 and 41.9 W $g_{Fe}^{-1}$) at lower concentrations of 0.5 and 1 mg mL$^{-1}$, respectively. Thus, on the basis of the faster heating profiles and higher SAR values, AFF-3 has been chosen for further studies.

*3.3.2. Effects of Applied Alternating Magnetic Fields (AMFs).* To study the effects of applied magnetic fields, AFF-3 (at 0.5–8 mg mL$^{-1}$ concentrations) has been exposed to AMFs with the amplitudes ($H$) and frequencies ($f$) in the range of 7.1–15.39 kA m$^{-1}$ and 175.2–1001.1 kHz, respectively (with $H \times f$ values ranging from 2.44 to 9.99 GAm$^{-1}$ s$^{-1}$, refer Table 2). The time taken by AFF-3 to reach the fixed/maximum temperature (≤45 °C) within the stipulated time of 30 min for the applied AMFs is correspondingly given in Table S3. It can be seen that the required time is reduced considerably with the increment of the AMFs (in terms of $H \times f$ values) to reach fixed/maximum temperature (≤45 °C). For instance, the time taken by AFF-3 (at 8 mg mL$^{-1}$ concentration) to reach 45 °C is reduced from 15.4 to 2.3 min with the increase in $H \times f$ values from 2.4 to 9.9 GAm$^{-1}$ s$^{-1}$. A similar reduction in time can be observed with the increase in $H \times f$ values for the other concentrations (i.e., 4, 2, 1, and 0.5 mg mL$^{-1}$) as well. Thus, the applied AMFs have a major influence in the heating rates of the SPIOs.

Furthermore, the calculated SAR values of AFF-3 for all of the applied AMFs are given in Table 2. It can be seen that the SAR values are decreased with the increase in the concentrations (i.e., from 0.5 to 8 mg mL$^{-1}$ concentration) in each of the applied magnetic fields. For instance, the SAR value has decreased from 165.8 to 32.3 with the increment in concentrations (from 0.5 to 8 mg mL$^{-1}$) for the $H \times f$ of 4.4 GAm$^{-1}$ s$^{-1}$. A similar decreasing trend is observed for the other $H \times f$ values as well, which could be mainly ascribed to more agglomerations at higher concentrations due to increased interparticle interactions between the SPIOs, which might have led to the formation of very long linear-chain structures inside the aqueous suspensions and subsequent reductions in their Brownian relaxations.[32−35]

Moreover, it can be noted that the SAR values are increasing with the increase in the applied magnetic field ($H \times f$ value) in each of the concentrations of the AFF-3. For instance, at 0.5 mg mL$^{-1}$ concentration of AFF-3 the following holds true: (i) if $H \times f <$ Hergt's limit (i.e., 5 GAm$^{-1}$ s$^{-1}$), the SAR values are estimated to be 48.6, 82.1, 100.5, 140.7, and 165.8 W $g_{Fe}^{-1}$ for the corresponding $H \times f$ values of 2.4, 3.4, 3.6, 4.1, and 4.4 GAm$^{-1}$ s$^{-1}$, respectively, and (ii) if $H \times f >$ Hergt's limit, the SAR values



DOI: 10.1021/acsomega.8b00207
ACS Omega 2018, 3, 3991−4005

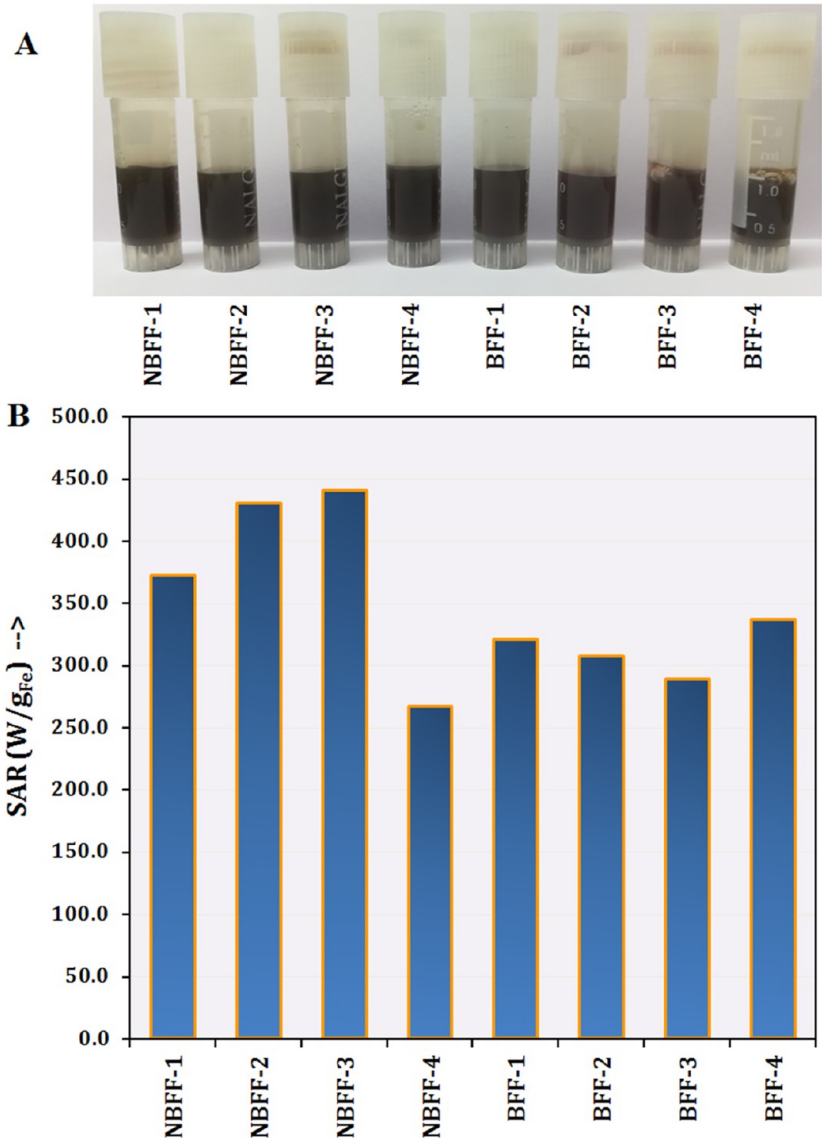


**Figure 6.** (A) 34DABA-coated SPIOs are dispersed in EG, DEG, TEG, GC, PBS, DMEM, DMEM + 5% FBS, and FBS with corresponding markings of NBFF-1, NBFF-2, NBFF-3, NBFF-4, BFF-1, BFF-2, BFF-3, and BFF-4. (B) SAR values of NBFF-1, NBFF-2, NBFF-3, NBFF-4, BFF-1, BFF-2, BFF-3, and BFF-4 at 0.5 mg $mL^{-1}$ concentration on exposure to AMF with $H \times f$ value of 8.2 $GAm^{-1}$ $s^{-1}$.

**Table 3. Mean Hydrodynamic Diameter ($D_h$, nm), SAR (W $g_{Fe}^{-1}$), and ILP ($nHm^2$ $kg^{-1}$) Values of 34DABA-Coated SPIOs Dispersed in Different Media**

| media type | FF code | media | density (g $cm^{-3}$) | specific heat capacity (J $kg^{-1}$ $K^{-1}$) | mean hydrodynamic diameter ($D_h$, nm) | SAR at 0.5 mg $mL^{-1}$ (W $g_{Fe}^{-1}$) | ILP at 0.5 mg $mL^{-1}$ ($nHm^2$ $kg^{-1}$) |
|---|---|---|---|---|---|---|---|
| aqueous | AFF-3 | water | 1.000 | 8374 | 193.5 | 330.8 | 3.7 |
| nonbiological (NBFFs) | NBFF-1 | EG | 1.115 | 4866 | 194.3 | 372.6 | 4.1 |
| | NBFF-2 | DEG | 1.118 | 4604 | 206.9 | 430.1 | 4.8 |
| | NBFF-3 | TEG | 1.125 | 4324 | 217.9 | 440.4 | 4.9 |
| | NBFF-4 | GC | 1.260 | 3086 | 237.4 | 266.9 | 3.0 |
| biological (BFFs) | BFF-1 | PBS | 1.000 | 8374 | 280.7 | 321.0 | 3.6 |
| | BFF-2 | DMEM | | | 388.2 | 307.0 | 3.4 |
| | BFF-3 | DMEM + 5% FBS | | | 370.6 | 288.9 | 3.2 |
| | BFF-4 | FBS | | | 226.9 | 336.9 | 3.7 |

are estimated to be 189.3, 330.8, and 432.1 W $g_{Fe}^{-1}$ for the corresponding $H \times f$ values of 8, 8.2, and 9.9 $GAm^{-1}$ $s^{-1}$ (calculated on the basis of the average of three readings to maintain repeatability/consistency at this concentration), respectively. Figure 5i shows the linear increasing trend in SAR values with the increment in $H \times f$ values (at 0.5 mg $mL^{-1}$ concentration of AFF-3), which is in good correlation with the reported literature.[36] The obtained SAR values of AFF-3 are



DOI: 10.1021/acsomega.8b00207
ACS Omega 2018, 3, 3991−4005

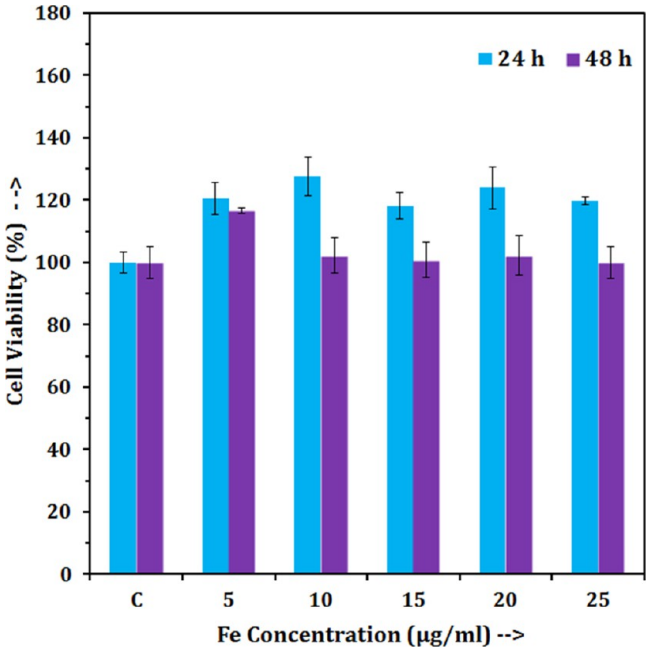


**Figure 7.** Cell viability plot of the SPIOs (34DABA-coated S3) at different concentrations (5−25 $\mu g_{Fe}$ per well) determined via trypan blue assay after 24 and 48 h incubation with HepG2 liver cancer cells. Label C indicates the control cells (i.e., without SPIOs).

higher than many already-reported SPIO-based AFFs (having similar physicochemical/magnetic properties) that are functionalized with short-chained and $\sigma$-conjugated surfactants. For instance, the SPIO-based AFFs that are coated with sodium oleate,[37] citric acid/albumin,[38] glycyrrhizic acid,[39] glycine,[40] and pentenoic acid[41] have exhibited respective SAR values of 14, 16.7, 17.9, 77.6, and 110.6 W $g_{Fe}^{-1}$ (which are lower than those values of AFF-3). In addition, AFF-3 (34DABA-coated SPIOs) has shown improved heating efficiency (or high SAR values) as compared to our previously reported AFFs that are prepared from the SPIOs having only carboxyl-based end groups.[18] The better heating efficiency of AFF-3 could be due to larger particle size and higher magnetic response of the SPIOs core to the applied AMFs via (i) enhanced $\pi-\pi$ conjugation paths of the surface-attached 34DABA coating molecules due to the intrafunctional group attractions from their close structural orientation (refer Scheme 1C(i)) (ii) improved anisotropy due to the formation of clusters/linear chains/loops of the SPIOs in the ferrofluids suspension due to the interfunctional group attractions (i.e., $-NH_2$ and $-COOH$ groups, refer Scheme 1C(ii)) and interparticle (i.e., particle−particle) interactions among different SPIOs (refer Scheme 1C(iii)) and their parallel alignment to the applied AMF.[35,42,43]

In addition, the ILP values (normalized SAR) of AFF-3 are calculated as per eq 2 for all of the concentrations for all $H \times f$ values (refer Table 2). The highest ILP value of 5.2 $nHm^2\ kg^{-1}$ is observed at 0.5 mg $mL^{-1}$ concentration and $H \times f = 4.4 \times 10^9$ $GAm^{-1}\ s^{-1}$ (i.e., below the Hergt's limit, refer Figure 5ii), which is larger than several commercially available SPIO-based FFs, for instance, 0.16, 0.17, 0.35, 1.71, and 2.31 $nHm^2\ kg^{-1}$ for BNF-0208, BNF-01808, BNF-01908, Fluidmag, and nanomag-D-spio, respectively.[44]

*3.3.3. Effects of Dispersion Media.* The dispersion media of the SPIO-based FFs might also have significant roles in influencing their heating responses by modifying the Néel/Brownian relaxation mechanisms. The heat generating effects of the SPIOs are studied in different biological/nonbiological carrier liquids (refer Figure 6A for nonbiological ferrofluids (NBFFs)/biological ferrofluids (BFFs)). Table 3 shows the heating efficacies (SAR/ILP values) of the NBFFs/BFFs at 0.5 mg $mL^{-1}$ concentration with an applied AMF ($H \times f$ = 8.2 $GAm^{-1}\ s^{-1}$), which is then compared by plotting their SAR values in Figure 6B.

It can be seen that all of the NBFFs have reached the therapeutic temperature (42−45 °C) similar to their aqueous counterpart (AFF-3) at 0.5 mg $mL^{-1}$ concentration within the stipulated time of 30 min. The SAR value is gradually increased from 330.8 W $g_{Fe}^{-1}$ (AFF-3) to 372.6/430.1 W $g_{Fe}^{-1}$ (NBFF-1/NBFF-2), reaching to a maximum value of 440.4 W $g_{Fe}^{-1}$ (NBFF-3) and then decreasing to 266.9 W $g_{Fe}^{-1}$ (NBFF-4), which is in good correlation with the results already reported in the literature.[45,46] The increment in the SAR values from NBFF-1 to NBFF-3 could be due to the increment of density of the carrier media of the NBFFs (refer Table 3). Besides, this increment could be associated with the slight aggregation of the SPIOs in the corresponding carrier liquids, as evident from the increment in their hydrodynamic sizes (refer Table 3). However, the SAR value is decreased for the NBFF-4 (regardless of its highest hydrodynamic size among all of the NBFFs), which could be mainly ascribed to the considerable reduction in its relaxation mechanisms due to near immobilization of the SPIOs in the highly viscous carrier liquid.

On the other hand, the SAR value is gradually decreased from 321 W $g_{Fe}^{-1}$ (BFF-1) to 307 W $g_{Fe}^{-1}$ (BFF-2), reaching to a minimum value of 288.9 W $g_{Fe}^{-1}$ (BFF-3), and then increased to 336.9 W $g_{Fe}^{-1}$ (BFF-4). The decrement in the SAR values from BFF-1 to BFF-3 could be due to the large aggregation of the SPIOs in the respective biological media, as apparent from the large increment in their hydrodynamic sizes (refer Table 3), attributed to the complex interactions between the surface-functional groups of the SPIOs and the carrier liquid molecules (glucose, phosphate, etc.).[47−52] But the BFF-4 exhibited the highest SAR value among all of the BFFs, which could be due to its lowest hydrodynamic size (refer Table 3).

In conclusion, the surface coatings, concentrations, applied alternating magnetic fields, and dispersion media have significant impacts on the heating efficiencies of the SPIOs/AFFs.

**3.4. Biological Studies.** *3.4.1. In Vitro Cell Viability.* In vitro cell viability of the 34DABA-coated SPIOs (S3/AFF-3) is determined in the HepG2 liver cancer cells via trypan blue assay by considering two incubation time periods (24/48 h) using the concentrations ranging from 5−25 $\mu g_{Fe}$ per well. The cytotoxicity results of the SPIOs are plotted against the control cells (i.e., without SPIOs), where the cell viability is considered as 100% (refer Figure 7). It can be noted that the HepG2 cells, treated with the SPIOs in all concentrations, display excellent viability at both 24 and 48 h incubation periods. Thus, the cell viability results indicate that the SPIOs are very biocompatible with the HepG2 cells. Besides, no morphological changes in HepG2 cancer cells are observed after 24 and 48 h incubation with S3 (at concentrations of 5−25 $\mu g_{Fe}$ per well), refer Figure 3A(i−vi) and B(i−vi), respectively.

*3.4.2. In Vitro MFH and WCTT.* Herein, the killing efficiency of the 34DABA-coated SPIOs (S3) in HepG2 cancer cells via MFH (at 42 °C) is determined and compared to that of the cells without MFH; i.e., the cells are treated with only AMF, water bath, and SPIOs. No considerable death (as per Figure 8A) is observed for the HepG2 cells that are treated with only magnetic



DOI: 10.1021/acsomega.8b00207
ACS Omega 2018, 3, 3991−4005

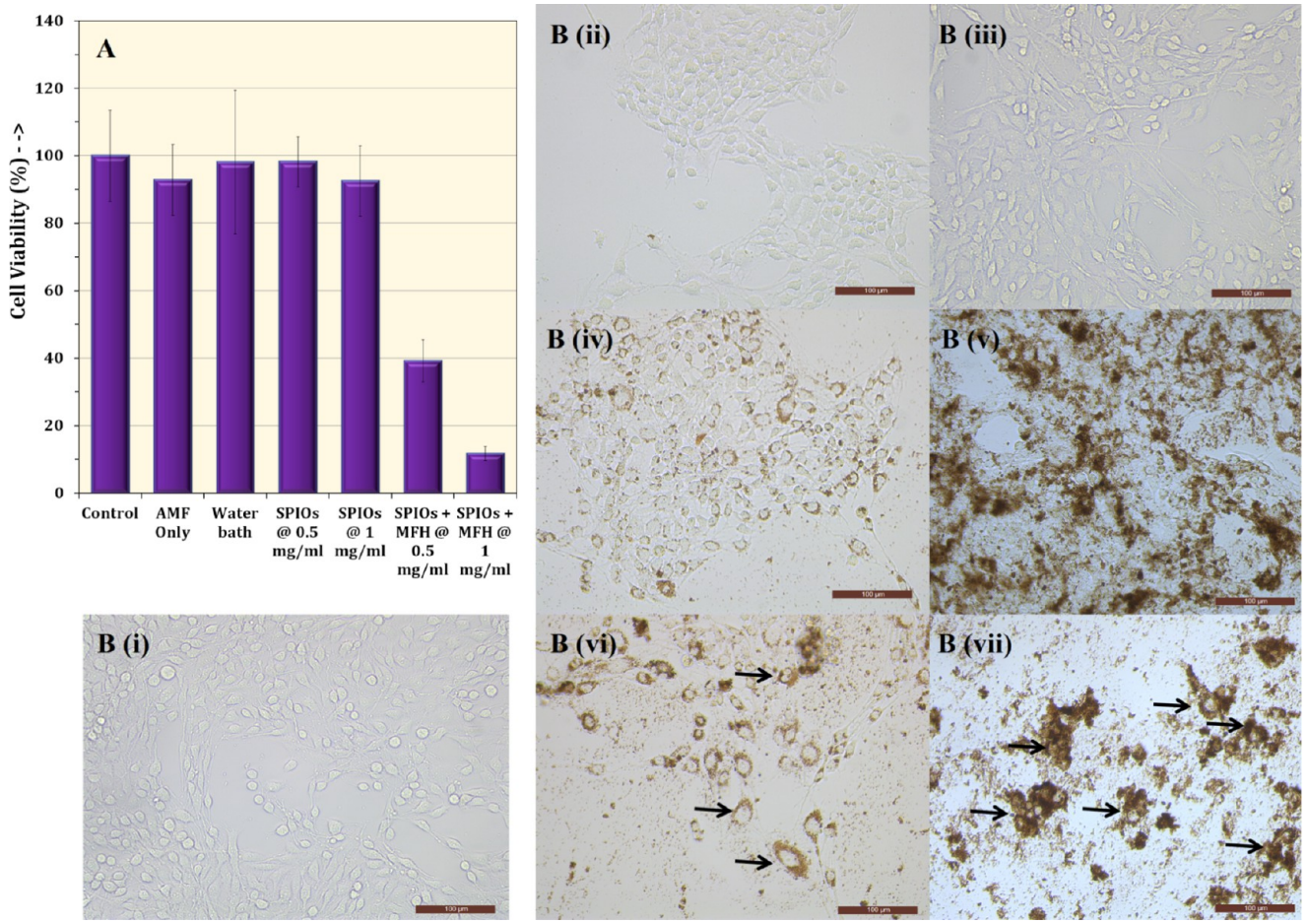


**Figure 8.** (A) Cell viability plot depicts the cytotoxic effect on HepG2 cancer cells treated with MFH (~42 °C) by using the SPIOs (34DABA-coated-S3) at 0.5 and 1 mg $mL^{-1}$ concentration on exposure to AMF (with $H \times f$ value of 8.2 $GAm^{-1}$ $s^{-1}$) as compared to control, cells treated with magnetic field only (i.e., without SPIOs), cells treated with water-bath only (i.e., without AMF and SPIOs), and cells incubated with SPIOs only (at 0.5 and 1 mg $mL^{-1}$ concentrations, without AMF/water bath). (B) Comparison of optical microscopic images (taken at 20× (i.e., 100 $\mu$m) magnification) of HepG2 liver cancer cells (i) control, (ii) cells treated with magnetic field only (i.e., without SPIOs), (iii) cells treated with water-bath only (i.e., without AMF and SPIOs), (iv, v) cells incubated with SPIOs only (i.e., without AMF/water bath) at 0.5 and 1 mg $mL^{-1}$ concentrations, respectively, and (vi, vii) cells treated with MFH by using SPIOs at 0.5 and 1 mg $mL^{-1}$ concentrations, respectively.

field (i.e., AMF) and water-bath-based thermotherapy (i.e., WCTT), as compared with the control, and moreover, no morphological changes are observed; refer Figure 8B(i–iii). However, the HepG2 cells that are treated with only S3 (i.e., without exposing to AMF) at 0.5 and 1 mg $mL^{-1}$ concentrations have exhibited very negligible cell death percentages, i.e., 2 and 8%, respectively (as per Figure 8A), and no considerable morphological changes are observed (refer Figure 8B(iv),(v)). But S3 has induced ~61 and ~88% cell death at 0.5 and 1 mg $mL^{-1}$ concentrations, respectively (as per Figure 8A) and considerable morphological changes in cells are observed after MFH treatment at 0.5 and 1 mg $mL^{-1}$ concentrations, indicated in black arrows in Figure 8B(vi),(vii), respectively. This indicates that S3 is capable of inducing high cancer cell death via MFH at 0.5/1 mg $mL^{-1}$ (lower) concentrations, which could be ascribed to its better heating responses under the applied AMF, as discussed in previous sections.

*3.4.3. In Vitro Uptake.* In vitro uptake of SPIOs (i.e., intracellular Fe ions) is qualitatively confirmed via the Prussian blue staining method. It can be noted from the microscopic images in Figure 9i,ii that the control cells (without and with AMF, respectively) have not displayed any blue staining. Moreover, the cells have displayed the blue staining when they are incubated with 34DABA-coated SPIOs (S3 at 15 $\mu g_{Fe}$) for 24 and 48 h (refer Figure 9iii,iv) during the cytotoxicity measurements. In addition, the HepG2 cells after the MFH (i.e., treated with SPIOs + AMF at 0.5 and 1 mg $mL^{-1}$ concentrations, refer Figure 9vii,viii, respectively) have shown relatively higher staining as compared with the cells that are treated with only SPIOs (i.e., no exposure to AMF, at 0.5 and 1 mg $mL^{-1}$ concentration, refer Figure 9v,vi, respectively). This indicates that the SPIOs are effectively uptaken by the HepG2 cells even at shorter time periods (during 1 h MFH treatment), resulting in higher percentages of the cancer cell death.

On the basis of the above biological results, it can be concluded that 34DABA-coated SPIOs are very efficient for in vitro MFH and thus could be used for cancer thermotherapies.

## 4. CONCLUSIONS

To summarize, we have successfully synthesized hydrophilic and functionalized SPIOs via one-pot facile co-precipitation/thermolysis methods using single surfactants (14DAB/4ABA/34DABA) and dual surfactants (combined with TA/ATA/TMA/PMA). The as-synthesized SPIOs are characterized for their physicochemical/magnetic/dispersibility properties. Although all of the SPIOs have exhibited superparamagnetic



DOI: 10.1021/acsomega.8b00207
*ACS Omega* 2018, 3, 3991–4005

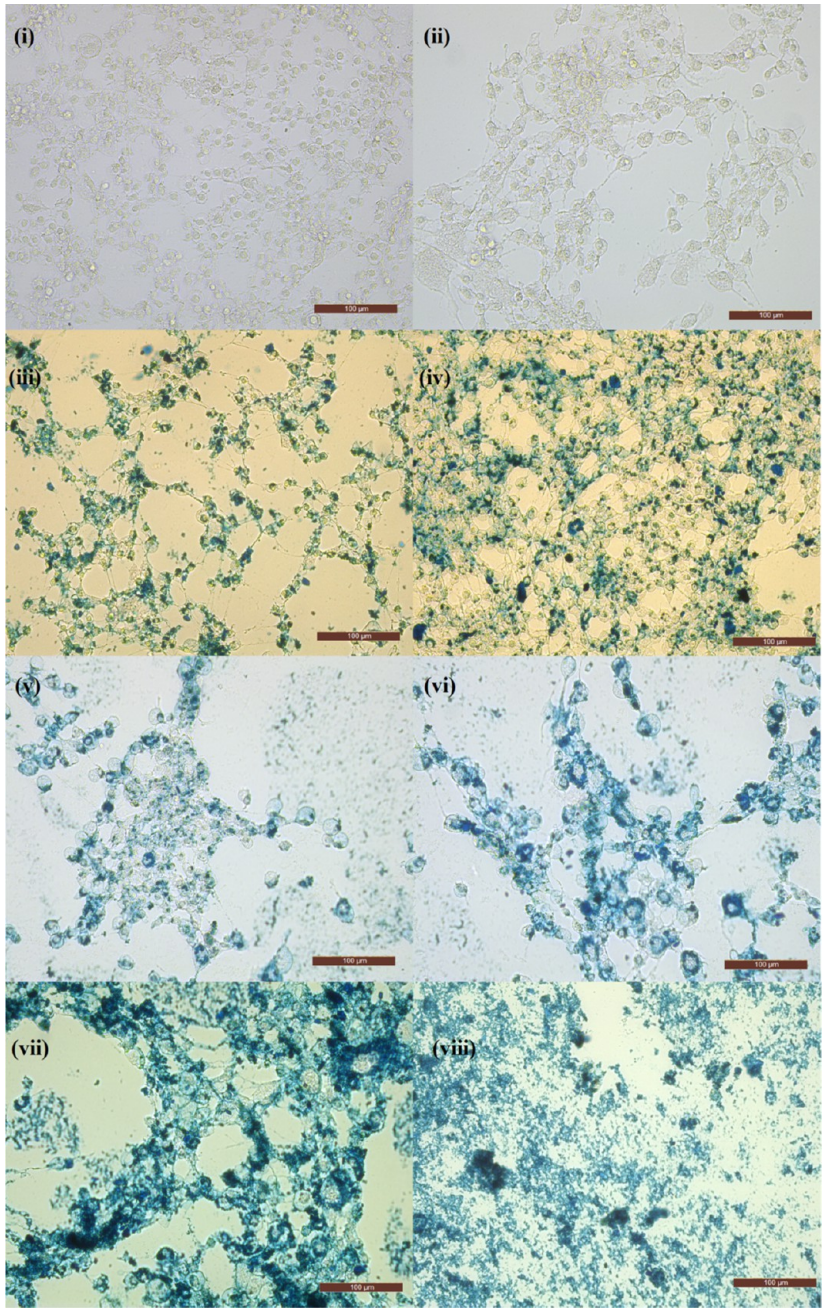


**Figure 9.** Comparison of optical microscopic images (taken at 20× (i.e., 100 $\mu$m) magnification) of HepG2 liver cancer cells after Prussian Blue staining: (i) control, (ii) cells treated with magnetic field only (i.e., without SPIOs), (iii, iv) cells incubated with SPIOs at 15 $\mu g_{Fe}$ per well after 24 and 48 h incubation, respectively, (v, vi) cells incubated with SPIOs at 0.5 and 1 mg $mL^{-1}$ concentrations, respectively, and (vii, viii) cells treated with MFH by using SPIOs at 0.5 and 1 mg $mL^{-1}$ concentrations, respectively.

behavior, only 14DAB-, 4ABA-, 34DABA-, and 4ABA-TA-coated SPIOs (S1, S2, S3, and S8 samples) have shown high magnetization values ($M_s$ = 55−71 emu $g^{-1}$). Besides, these SPIOs are found to be spherical in shape with their TEM and DLS sizes in the range of 6−10 nm and 137−193 nm, respectively. In addition, they have displayed good water dispersibility with high $\zeta$-potential values (−31 to −43 mV). In calorimetric MFH (C-MFH) studies, the aqueous ferrofluids (AFF-1−AFF-4) have displayed excellent time-dependent temperature rise under the application of external magnetic fields. The AFF-3 (i.e., 34DABA-coated SPIOs) has revealed faster thermal response to the AMF and reached the therapeutic temperature even at the lowest concentration (0.5 mg $mL^{-1}$) as compared to AFF-1, AFF-2, and AFF-4. Moreover, AFF-3 has exhibited high heating efficacies with SAR and ILP values of 48−432 W $g_{Fe}^{-1}$ and 0.6−5.2 $nHm^2\ kg^{-1}$, respectively, with the AMF frequencies ranging from 175 to 1001 kHz. Besides, the high viscous TEG-based ferrofluids (NBFF-3, with 34DABA-coated SPIOs) exhibited the highest SAR value (440.4 W $g_{Fe}^{-1}$) and also reached therapeutic temperatures at a faster rate as compared to their counterparts in other biological and nonbiological media. Moreover, the 34DABA-coated SPIOs have (i) demonstrated very good cytocompatibility (without MFH) and (ii) achieved higher killing efficiency of ∼61 and ∼88% (with MFH) in a concentration-dependent manner (i.e., for 0.5 and 1 mg $mL^{-1}$, respectively) in HepG2 cancer cells as compared with their


DOI: 10.1021/acsomega.8b00207
*ACS Omega* 2018, 3, 3991−4005

treatment with only magnetic field/SPIOs and water-bath-based conventional thermotherapy (i.e., without SPIOs/MFH). Besides, the incubated 34DABA-coated SPIOs are effectively internalized by the HepG2 liver cancer cells during cytotoxicity and in vitro MFH experiments, as confirmed via Prussian blue staining. Hence, the as-synthesized 34DABA-coated SPIOs are very promising heat-inducing agents for the MFH and could be efficiently used as nanomedicines for the cancer thermotherapy.

## ■ ASSOCIATED CONTENT

### Supporting Information

The Supporting Information is available free of charge on the ACS Publications website at DOI: 10.1021/acsomega.8b00207.

Tables of reaction conditions, TGA secondary weight losses, and saturation magnetization values for the as-synthesized SPIOs, and calorimetric MFH data including SAR and ILP values for the as-prepared FFs; figures of TGA and VSM curves for the as-synthesized SPIOs, and the microscopic images of HepG2 cancer cells after 24 and 48 h incubation with 34DABA-coated SPIOs (PDF)

## ■ AUTHOR INFORMATION


### Corresponding Author

*E-mail: dipak.maity@snu.edu.in.

### ORCID

Ganeshlenin Kandasamy: 0000-0002-6849-6538

Dipak Maity: 0000-0001-9792-0281


### Notes

The authors declare no competing financial interest.

## ■ ACKNOWLEDGMENTS

The authors gratefully acknowledge Dr. Anindita Chakrabarty (Department of Life Sciences, Shiv Nadar University, India), Dr. Subhabrata Sen, and Dr. Gouriprasanna Roy (Department of Chemistry, Shiv Nadar University, India) either for providing the cell culture facilities or fruitful discussions. The authors also wish to thank Dr. Manoj Kumar, Malaviya National Institute of Technology, Jaipur, India for providing TGA facility and USIC, University of Delhi, for providing TEM and TGA facilities. Moreover, the financial supports received from (i) Nanomission (Grant No. SR/NM/NS-1141/2015 (G)), Department of Science and Technology (DST), New Delhi, India and (ii) Shiv Nadar University, Uttar Pradesh, India are appreciatively acknowledged.

## ■ REFERENCES


(1) Praetorius, N. P.; Mandal, T. K. Engineered Nanoparticles in Cancer Therapy. *Recent Pat. Drug Delivery Formulation* **2007**, *1*, 37−51.

(2) Kumar, C. S. S. R.; Mohammad, F. Magnetic Nanomaterials for Hyperthermia-Based Therapy and Controlled Drug Delivery. *Adv. Drug Delivery Rev.* **2011**, *63*, 789−808.

(3) Laurent, S.; Mahmoudi, M. Superparamagnetic Iron Oxide Nanoparticles: Promises for Diagnosis and Treatment of Cancer. *Int. J. Mol. Epidemiol. Genet.* **2011**, *2*, 367−390.

(4) Wahajuddin; Arora, S. Superparamagnetic Iron Oxide Nanoparticles: Magnetic Nanoplatforms as Drug Carriers. *Int. J. Nanomed.* **2012**, *7*, 3445−3471.

(5) Li, W.; Zaloga, J.; Ding, Y.; Liu, Y.; Janko, C.; Pischetsrieder, M.; Alexiou, C.; Boccaccini, A. R. Facile Preparation of Multifunctional Superparamagnetic PHBV Microspheres Containing SPIONs for Biomedical Applications. *Sci. Rep.* **2016**, *6*, No. 23140.

(6) Mikhaylova, M.; Kim, D. K.; Bobrysheva, N.; Osmolowsky, M.; Semenov, V.; Tsakalakos, T.; Muhammed, M. Superparamagnetism of Magnetite Nanoparticles: Dependence on Surface Modification. *Langmuir* **2004**, *20*, 2472−2477.

(7) Maity, D.; Kandasamy, G.; Sudame, A. Superparamagnetic Iron Oxide Nanoparticles (SPIONs) Based Magnetic Hyperthermia: A Promising Therapy in Cancer Treatment. In *Advances in Medicine and Biology*; Berhardt, L. V., Ed.; Nova Science Publishers, 2017; pp 99−160.

(8) Mornet, S.; Vasseur, S.; Grasset, F.; Duguet, E. Magnetic Nanoparticle Design for Medical Diagnosis and Therapy. *J. Mater. Chem.* **2004**, *14*, 2161−2175.

(9) Kandasamy, G.; Maity, D. Recent Advances in Superparamagnetic Iron Oxide Nanoparticles (SPIONs) for in Vitro and in Vivo Cancer Nanotheranostics. *Int. J. Pharm.* **2015**, *496*, 191−218.

(10) Chandrasekharan, P.; Maity, D.; Yong, C. X.; Chuang, K. H.; Ding, J.; Feng, S. S. Vitamin E (D-Alpha-Tocopheryl-Co-Poly(ethylene Glycol) 1000 Succinate) Micelles-Superparamagnetic Iron Oxide Nanoparticles for Enhanced Thermotherapy and MRI. *Biomaterials* **2011**, *32*, 5663−5672.

(11) Lam, T.; Pouliot, P.; Avti, P. K.; Lesage, F.; Kakkar, A. K. Superparamagnetic Iron Oxide Based Nanoprobes for Imaging and Theranostics. *Adv. Colloid Interface Sci.* **2013**, *199*−*200*, 95−113.

(12) Martinez-Boubeta, C.; Simeonidis, K.; Makridis, A.; Angelakeris, M.; Iglesias, O.; Guardia, P.; Cabot, A.; Yedra, L.; Estradé, S.; Peiró, F.; Saghi, Z.; Midgley, P.; Conde-Leborán, I.; Serantes, D.; Baldomir, D. Learning from Nature to Improve the Heat Generation of Iron-Oxide Nanoparticles for Magnetic Hyperthermia Applications. *Sci. Rep.* **2013**, *3*, No. 1652.

(13) Lartigue, L.; Hugounenq, P.; Alloyeau, D.; Clarke, S. P.; Lévy, M.; Bacri, J. C.; Bazzi, R.; Brougham, D. F.; Wilhelm, C.; Gazeau, F. Cooperative Organization in Iron Oxide Multi-Core Nanoparticles Potentiates Their Efficiency as Heating Mediators and MRI Contrast Agents. *ACS Nano* **2012**, *6*, 10935−10949.

(14) Guardia, P.; Corato, R. D.; Lartigue, L.; Wilhelm, C.; Espinosa, A.; Garcia-Hernandez, M.; Gazeau, F.; Manna, L.; Pellegrino, T. Water Soluble Iron Oxide Nanocubes with High Values of Specific Absorption Rate for Cancer Cell Hyperthermia Treatment. *ACS Nano* **2012**, *6*, 3080−3091.

(15) de la Presa, P.; Luengo, Y.; Multigner, M.; Costo, R.; Morales, M. P.; Rivero, G.; Hernando, A. Study of Heating Efficiency as a Function of Concentration, Size, and Applied Field in $\gamma$-Fe2O3 Nanoparticles. *J. Phys. Chem. C* **2012**, *116*, 25602−25610.

(16) Bae, K. H.; Park, M.; Do, M. J.; Lee, N.; Ryu, J. H.; Kim, G. W.; Kim, C.; Park, T. G.; Hyeon, T. Chitosan Oligosaccharide-Stabilized Ferrimagnetic Iron Oxide Nanocubes for Magnetically Modulated Cancer Hyperthermia. *ACS Nano* **2012**, *6*, 5266−5273.

(17) Lahiri, B. B.; Ranoo, S.; Zaibudeen, A. W.; Philip, J. Magnetic Hyperthermia in Magnetic Nanoemulsions: Effects of Polydispersity, Particle Concentration and Medium Viscosity. *J. Magn. Magn. Mater.* **2017**, *441*, 310−327.

(18) Kandasamy, G.; Sudame, A.; Bhati, P.; Chakrabarty, A.; Kale, S. N.; Maity, D. Systematic Magnetic Fluid Hyperthermia Studies of Carboxyl Functionalized Hydrophilic Superparamagnetic Iron Oxide Nanoparticles Based Ferrofluids. *J. Colloid Interface Sci.* **2018**, *514*, 534−543.

(19) Kandasamy, G.; Surendran, S.; Chakrabarty, A.; Kale, S. N.; Maity, D. Facile Synthesis of Novel Hydrophilic and Carboxyl-Amine Functionalized Superparamagnetic Iron Oxide Nanoparticles for Biomedical Applications. *RSC Adv.* **2016**, *6*, 99948−99959.

(20) Das, M.; Mishra, D.; Dhak, P.; Gupta, S.; Maiti, T. K.; Basak, A.; Pramanik, P. Biofunctionalized, Phosphonate-Grafted, Ultrasmall Iron Oxide Nanoparticles for Combined Targeted Cancer Therapy and Multimodal Imaging. *Small* **2009**, *5*, 2883−2893.

(21) Maity, D.; Chandrasekharan, P.; Yang, C.-T.; Chuang, K.-H.; Shuter, B.; Xue, J.-M.; Ding, J.; Feng, S.-S. Facile Synthesis of Water-Stable Magnetite Nanoparticles for Clinical MRI and Magnetic Hyperthermia Applications. *Nanomedicine* **2010**, *5*, 1571−1584.

(22) Maity, D.; Pradhan, P.; Chandrasekharan, P.; Kale, S. N.; Shuter, B.; Bahadur, D.; Feng, S.-S.; Xue, J.-M.; Ding, J. Synthesis of Hydrophilic Superparamagnetic Magnetite Nanoparticles via Thermal Decomposi-




DOI: 10.1021/acsomega.8b00207
*ACS Omega* 2018, 3, 3991−4005

tion of Fe(acac)3 in 80 Vol% TREG + 20 Vol% TREM. *J. Nanosci. Nanotechnol.* **2011**, *11*, 2730−2734.
(23) Maity, D.; Chandrasekharan, P.; Pradhan, P.; Chuang, K.-H.; Xue, J.-M.; Feng, S.-S.; Ding, J. Novel Synthesis of Superparamagnetic Magnetite Nanoclusters for Biomedical Applications. *J. Mater. Chem.* **2011**, *21*, 14717.
(24) Nigam, S.; Bahadur, D. Dendrimer-Conjugated Iron Oxide Nanoparticles as Stimuli-Responsive Drug Carriers for Thermally-Activated Chemotherapy of Cancer. *Colloids Surf., B* **2017**, *155*, 182−192.
(25) Pierce, Z.; Strawbridge, R.; Gaito, C.; Dulatas, L.; Tate, J.; Ogden, J.; Hoopes, P. J. In-Vitro Investigations of Nanoparticle Magnetic Thermotherapy: Adjuvant Effects and Comparison to Conventional Heating. *Proc. SPIE-Int. Soc. Opt. Eng.* **2007**, *6440*, No. 64400J.
(26) Cai, H.; An, X.; Cui, J.; Li, J.; Wen, S.; Li, K.; Shen, M.; Zheng, L.; Zhang, G.; Shi, X. Facile Hydrothermal Synthesis and Surface Functionalization of Polyethyleneimine-Coated Iron Oxide Nanoparticles for Biomedical Applications. *ACS Appl. Mater. Interfaces* **2013**, *5*, 1722−1731.
(27) Maity, D.; Kale, S. N.; Kaul-Ghanekar, R.; Xue, J.-M.; Ding, J. Studies of Magnetite Nanoparticles Synthesized by Thermal Decomposition of Iron (III) Acetylacetonate in Tri(ethylene Glycol). *J. Magn. Magn. Mater.* **2009**, *321*, 3093−3098.
(28) Ilyas, S.; Ilyas, M.; van der Hoorn, R. A. L.; Mathur, S. Selective Conjugation of Proteins by Mining Active Proteomes through Click-Functionalized Magnetic Nanoparticles. *ACS Nano* **2013**, *7*, 9655−9663.
(29) Kossatz, S.; Grandke, J.; Couleaud, P.; Latorre, A.; Aires, A.; Crosbie-Staunton, K.; Ludwig, R.; Dähring, H.; Ettelt, V.; Lazaro-Carrillo, A.; Calero, M.; Sader, M.; Courty, J.; Volkov, Y.; Prina-Mello, A.; Villanueva, A.; Somoza, Á.; Cortajarena, A. L.; Miranda, R.; Hilger, I. Efficient Treatment of Breast Cancer Xenografts with Multifunctionalized Iron Oxide Nanoparticles Combining Magnetic Hyperthermia and Anti-Cancer Drug Delivery. *Breast Cancer Res.* **2015**, *17*, 66.
(30) Shubitidze, F.; Kekalo, K.; Stigliano, R.; Baker, I. Magnetic Nanoparticles with High Specific Absorption Rate of Electromagnetic Energy at Low Field Strength for Hyperthermia Therapy. *J. Appl. Phys.* **2015**, *117*, No. 094302.
(31) Pearce, J.; Giustini, A.; Stigliano, R.; Jack Hoopes, P. Magnetic Heating of Nanoparticles: The Importance of Particle Clustering to Achieve Therapeutic Temperatures. *J. Nanotechnol. Eng. Med.* **2013**, *4*, No. 011005.
(32) Lahiri, B. B.; Muthukumaran, T.; Philip, J. Magnetic Hyperthermia in Phosphate Coated Iron Oxide Nanofluids. *J. Magn. Magn. Mater.* **2016**, *407*, 101−113.
(33) Guibert, C.; Dupuis, V.; Peyre, V.; Fresnais, J. Hyperthermia of Magnetic Nanoparticles: Experimental Study of the Role of Aggregation. *J. Phys. Chem. C* **2015**, *119*, 28148−28154.
(34) Lahiri, B. B.; Ranoo, S.; Philip, J. Magnetic Hyperthermia Study in Water Based Magnetic Fluids Containing TMAOH Coated Fe3O4 Using Infrared Thermography. *Infrared Phys. Technol.* **2017**, *80*, 71−82.
(35) Maity, D.; Agrawal, D. C. Synthesis of Iron Oxide Nanoparticles under Oxidizing Environment and Their Stabilization in Aqueous and Non-Aqueous Media. *J. Magn. Magn. Mater.* **2007**, *308*, 46−55.
(36) Rosensweig, R. E. E. Heating Magnetic Fluid with Alternating Magnetic Field. *J. Magn. Magn. Mater.* **2002**, *252*, 370−374.
(37) Araújo-Neto, R. P.; Silva-Freitas, E. L.; Carvalho, J. F.; Pontes, T. R. F.; Silva, K. L.; Damasceno, I. H. M.; Egito, E. S. T.; Dantas, A. L.; Morales, M. A.; Carriço, A. S. Monodisperse Sodium Oleate Coated Magnetite High Susceptibility Nanoparticles for Hyperthermia Applications. *J. Magn. Magn. Mater.* **2014**, *364*, 72−79.
(38) Cheraghipour, E.; Javadpour, S. Cationic Albumin-Conjugated Magnetite Nanoparticles, Novel Candidate for Hyperthermia Cancer Therapy. *Int. J. Hyperthermia* **2013**, *29*, 511−519.
(39) Saeedi, M.; Vahidi, O.; Bonakdar, S. Synthesis and Characterization of Glycyrrhizic Acid Coated Iron Oxide Nanoparticles for Hyperthermia Applications. *Mater. Sci. Eng., C* **2017**, *77*, 1060−1067.
(40) Barick, K. C.; Hassan, P. A. Glycine Passivated Fe3O4 Nanoparticles for Thermal Therapy. *J. Colloid Interface Sci.* **2012**, *369*, 96−102.
(41) Darwish, M. S. A.; Stibor, I. Pentenoic Acid-Stabilized Magnetic Nanoparticles for Nanomedicine Applications. *J. Dispersion Sci. Technol.* **2016**, *37*, 1793−1798.
(42) Jordan, A.; Wust, P.; Fähling, H.; John, W.; Hinz, A.; Felix, R. Inductive Heating of Ferrimagnetic Particles and Magnetic Fluids: Physical Evaluation of Their Potential for Hyperthermia. *Int. J. Hyperthermia* **1993**, *9*, 51−68.
(43) Kettering, M.; Grau, I.; Pömpner, N.; Stapf, M.; Gajda, M.; Teichgräber, U.; Hilger, I. Means to Increase the Therapeutic Efficiency of Magnetic Heating of Tumors. *Biomed. Eng.* **2015**, *60*, 505−517.
(44) Kallumadil, M.; Tada, M.; Nakagawa, T.; Abe, M.; Southern, P.; Pankhurst, Q. Suitability of Commercial Colloids for Magnetic Hyperthermia. *J. Magn. Magn. Mater.* **2009**, *321*, 1509−1513.
(45) Fortin, J.-P.; Wilhelm, C.; Servais, J.; Ménager, C.; Bacri, J.-C.; Gazeau, F. Size-Sorted Anionic Iron Oxide Nanomagnets as Colloidal Mediators for Magnetic Hyperthermia. *J. Am. Chem. Soc.* **2007**, *129*, 2628−2635.
(46) Chen, S.; Chiang, C.-l.; Hsieh, S. Simulating Physiological Conditions to Evaluate Nanoparticles for Magnetic Fluid Hyperthermia (MFH) Therapy Applications. *J. Magn. Magn. Mater.* **2010**, *322*, 247−252.
(47) Etheridge, M. L.; Hurley, K. R.; Zhang, J.; Jeon, S.; Ring, H. L.; Hogan, C.; Haynes, C. L.; Garwood, M.; Bischof, J. C. Accounting for Biological Aggregation in Heating and Imaging of Magnetic Nanoparticles. *Technology* **2014**, *2*, 214−228.
(48) Ovejero, J. G.; Cabrera, D.; Carrey, J.; Valdivielso, T.; Salas, G.; Teran, F. J. Effects of Inter- and Intra-Aggregate Magnetic Dipolar Interactions on the Magnetic Heating Efficiency of Iron Oxide Nanoparticles. *Phys. Chem. Chem. Phys.* **2016**, *18*, 10954−10963.
(49) Cabrera, D.; Camarero, J.; Ortega, D.; Teran, F. J. Influence of the Aggregation, Concentration, and Viscosity on the Nanomagnetism of Iron Oxide Nanoparticle Colloids for Magnetic Hyperthermia. *J. Nanopart. Res.* **2015**, *17*, No. 121.
(50) Soares, P. I. P.; Lochte, F.; Echeverria, C.; Pereira, L. C. J.; Coutinho, J. T.; Ferreira, I. M. M.; Novo, C. M. M.; Borges, J. P. M. R. Thermal and Magnetic Properties of Iron Oxide Colloids: Influence of Surfactants. *Nanotechnology* **2015**, *26*, No. 425704.
(51) Lévy, M.; Wilhelm, C.; Siaugue, J.-M.; Horner, O.; Bacri, J.-C.; Gazeau, F. Magnetically Induced Hyperthermia: Size-Dependent Heating Power of $\gamma$-Fe(2)O(3) Nanoparticles. *J. Phys.: Condens. Matter* **2008**, *20*, No. 204133.
(52) Conde-Leboran, I.; Baldomir, D.; Martinez-Boubeta, C.; Chubykalo-Fesenko, O.; del Puerto Morales, M.; Salas, G.; Cabrera, D.; Camarero, J.; Teran, F. J.; Serantes, D. A Single Picture Explains Diversity of Hyperthermia Response of Magnetic Nanoparticles. *J. Phys. Chem. C* **2015**, *119*, 15698−15706.



DOI: 10.1021/acsomega.8b00207
*ACS Omega* 2018, 3, 3991−4005